iScience

CellPress
OPEN ACCESS

Article

From biological data to oscillator models using SINDy

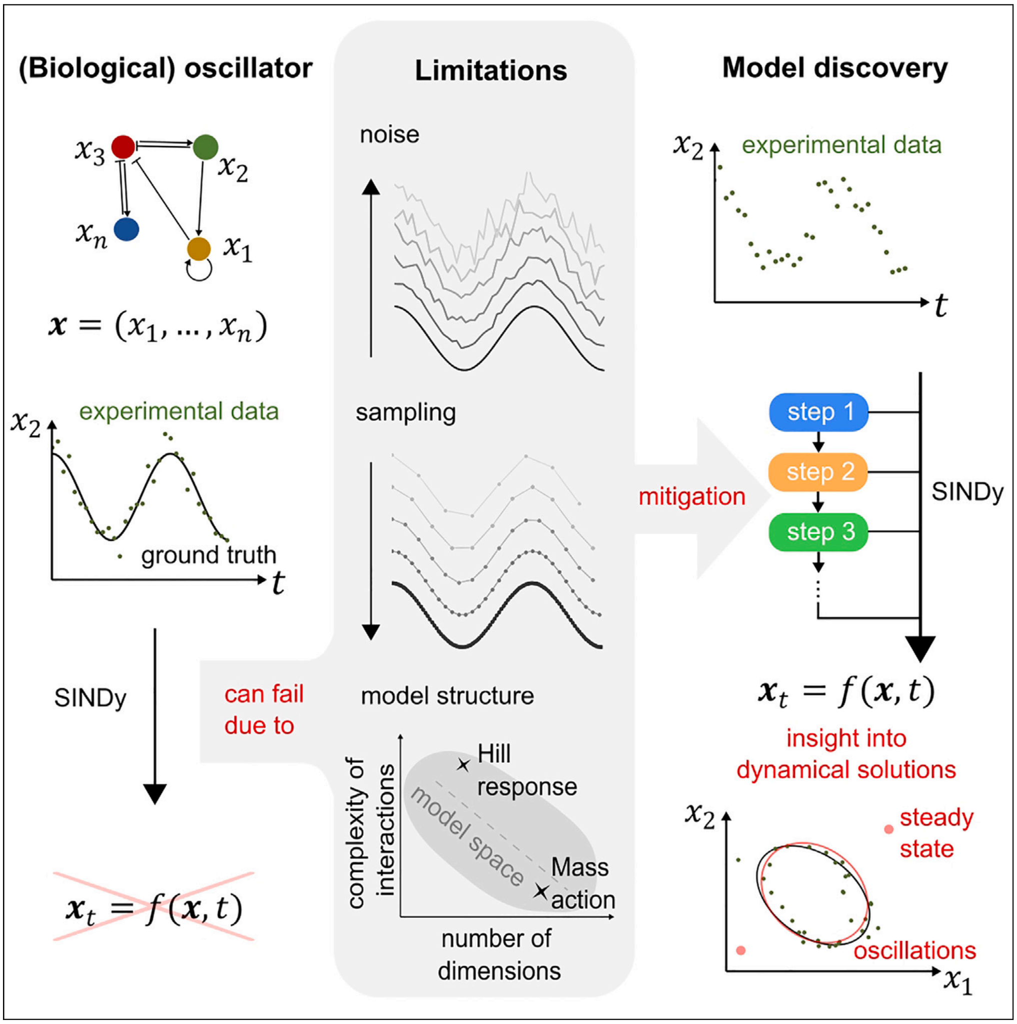

Bartosz Prokop, Lendert Gelens

bartosz.prokop@kuleuven.be (B.P.)
lendert.gelens@kuleuven.be (L.G.)

Highlights

SINDy struggles to discover models from low-quality experimental biological data

Existing SINDy extensions fail for time-scale separation in oscillations

A developed step-by-step guide helps experimentalists to successfully apply SINDy

Applying this guide leads to new models and insights into glycolytic oscillations

Prokop & Gelens, iScience *27*, 109316
April 19, 2024 © 2024 The Author(s).
https://doi.org/10.1016/j.isci.2024.109316

iScience

CellPress
OPEN ACCESS

Article

From biological data to oscillator models using SINDy

Bartosz Prokop[1,2,*] and Lendert Gelens[1,*]

SUMMARY

Periodic changes in the concentration or activity of different molecules regulate vital cellular processes such as cell division and circadian rhythms. Developing mathematical models is essential to better understand the mechanisms underlying these oscillations. Recent data-driven methods like SINDy have fundamentally changed model identification, yet their application to experimental biological data remains limited. This study investigates SINDy's constraints by directly applying it to biological oscillatory data. We identify insufficient resolution, noise, dimensionality, and limited prior knowledge as primary limitations. Using various generic oscillator models of different complexity and/or dimensionality, we systematically analyze these factors. We then propose a comprehensive guide for inferring models from biological data, addressing these challenges step by step. Our approach is validated using glycolytic oscillation data from yeast.

INTRODUCTION

Many important physical, chemical, and biological systems are characterized by periodic changes, also called oscillations. Examples of such oscillatory systems are in physics the mechanical pendulum or alternating current, in chemistry the Belousov-Zhabotinsky (BZ)[1,2] or Briggs-Rauscher[3] reactions, and in biology circadian rhythms,[4] population dynamics,[5,6] or the early embryonic cell cycle.[7]

Because of their ubiquity in a wide variety of systems, scientists have long been interested in understanding the underlying processes that describe and regulate the observed periodic behavior. To do this, they often use the language of mathematical models in the form of differential equations that can describe and predict the dynamics of a system. Such models are usually derived through experimental work, first principles, and/or scientific intuition.[8]

Prominent examples are the derivation of the simple pendulum model from observation and first principles described by Huygens[9] and later by Newton,[10] or the identification of the underlying mechanism of the BZ reaction by Field, Kórós, and Noyes[2] and the formulation of the Oregonator model.[11]

Design principles of biological oscillators

As in biology, the biochemical regulatory network is typically not completely characterized; it is difficult to derive model equations from first principles. However, biological oscillators have also been found to follow a few key design principles.[12] To date, all biological oscillators have three properties: **negative feedback**, **time delay**, and **nonlinearity**. Negative feedback is crucial to reset the system to its starting point after one oscillation period. Moreover, this feedback needs to be sufficiently time-delayed, and the interactions must be sufficiently nonlinear, to avoid the system getting stuck in a stable steady state.

By combining these basic design principles with experimental measurements, many mathematical models have been constructed that are capable of describing biochemical oscillatory processes. However, there exist many different ways to incorporate the three key properties that are required to ensure oscillations. A time-delayed negative feedback can be implemented explicitly by including a time delay in the equations, leading to delay differential equations, which are mathematically quite difficult to study. Examples include the Mackey-Glass model for the variation of CO_2 levels in blood[13] and the tumor suppressor protein p53 in response to DNA damage.[14] Another way to include a time delay is to introduce many intermediate steps (thus increasing the dimensionality of the system), which is how time delays result in mass action type models[15,16] or for simpler formulations as in the FitzHugh-Nagumo[17,18] and Goodwin models[19,20] by the strength of nonlinear coupling of state variable equations in the system. Also, where the negative feedback is implemented can vary; it can e.g., act on the production of the oscillating variable, or on its degradation.[21,22] Furthermore, nonlinearity can be incorporated directly, either in the form of higher order polynomial terms (as in the FitzHugh-Nagumo model[17,18]), or nonlinear expressions such as ultrasensitivity in the form of Hill functions (as in the Goodwin model[19,20]), or by increasing the amount of state variables (or dimensions) of a model (as in mass action type models[23,24]).

[1]Laboratory of Dynamics in Biological Systems, Department of Cellular and Molecular Medicine, KU Leuven, Herestraat 49, 3000 Leuven, Belgium
[2]Lead contact
*Correspondence: bartosz.prokop@kuleuven.be (B.P.), lendert.gelens@kuleuven.be (L.G.)
https://doi.org/10.1016/j.isci.2024.109316

This illustrates that formulating models using a combination of design principles, scientific intuition, and experimental measurements can potentially lead to ambiguous model formulations where the choice of specific model terms may be biased toward the scientist's preference. Furthermore, in the era of big data in biology identifying underlying patterns and formulating such models 'by hand' may become increasingly difficult or impossible.[25,26]

Data-driven model inference in biology

The recent emergence of data-driven methods, also called machine learning, has enabled the identification of such patterns in large datasets.[27] Such methods can be divided into two main types[28]: (1) *Black-box* methods that are trained on known data and are capable of predicting future outcomes, but do not provide interpretable models (model-free inference) and (2) *White-box* methods, which aim for interpretability and provide explicit mathematical models directly from data (model-based inference).

The focus of research in systems biology lies mostly in the identification of network structures,[29] such as gene transcription networks or protein-protein interaction networks. Here, one typically uses expression data, applying black-box methods based on neural networks[30] (e.g., graph neural networks[31]) or spectral methods[29] (e.g., GOBI[32]). With these methods it is possible to understand the underlying structures of a biological system, e.g., causal interactions,[33] but not the actual nature of interactions which lead to e.g., temporal oscillatory behavior.

To address the issue of interpretability while exploiting the ability of black-box approaches to identify patterns in measured data, mixed methods, also called gray-box approaches, have been developed. Examples of such methods include e.g., Physics-Informed Neural Networks in physics[34–36] or similarly termed Biologically Informed Neural Networks in biology,[37] which aim to improve interpretability of results by integrating prior knowledge into the design of trained neural networks. Other methods translate the structure of neural networks into interpretable mathematical equations via symbolic methods. For example, 'Symbolic Deep Learning'[38] aims at achieving this on the entire dynamical system, while 'Universal Differential Equations'[39] use neural networks only as a means to describe the most intricate, unknown parts of a dynamical system.

However, the simplest and most straightforward methods are white-box applications which are able to provide models of dynamical systems directly from data. Such methods are mainly regression-based and their prominent representatives are the 'Nonlinear Autoregressive Moving Average Model with Exogenous Inputs' (NARMAX),[40] 'Symbolic Regression'[41] and 'Sparse Identification of Nonlinear Dynamics' (SINDy).[42]

Especially SINDy has recently gained popularity in physics,[43,44] engineering,[45] chemistry[46] and biology[47,48] where it has shown great potential when applied on synthetic data. However, the SINDy method has been scarcely applied to real data. Examples include data from generic systems,[48,49] settlement data,[50] gene expression data[51] and mainly experimental data from predator-prey dynamics,[52–54] where SINDy was able to identify relevant aspects of the respective biological systems.

Structure of this work

Here, we aim to determine why the original SINDy is not (yet) often used on (biological) experimental data (beyond predator-prey dynamics), with a particular focus on biological oscillatory systems. We start by 'naively' applying SINDy to three selected, experimental datasets of oscillatory systems. We do so considering limited prior knowledge, no noise filtering, and using RIDGE regression similarly to the original publication by Brunton et al.[42]). We explore the simple pendulum, the chemical oscillations of the BZ reaction, and measurements of glycolytic oscillations in yeast. This allows us to define the main limiting aspects of the SINDy method. We then investigate these limitations using a set of commonly used, generic oscillator models varying in complexity and/or dimensionality: the FitzHugh-Nagumo model, the Goodwin model, and a mass action type model of the cell cycle. Based on this study, we formulate specific mitigation approaches and propose a step-by-step guide for model identification of dynamic (oscillatory) systems in biology using SINDy or other regression-based data-driven methods. Finally, we apply our guide to the introduced example of glycolytic oscillations in yeast.

RESULTS

Application of SINDy to experimental data

Before applying SINDy to experimental data, we briefly explain how we approach such model identification (see Figure 1).

We start by acquiring either new or existing data from the literature on an oscillatory system (see Figure 1A). Using a single, measured time series of all available variables, we generate the target vector X (more precisely the time derivative X_t) of all variables and propose a suitable term library $\boldsymbol{\Theta}$ containing all terms to be evaluated (see Figure 1B, all libraries used in this manuscript can be found in the table in the E-SINDy extension in the STAR Methods). This term library thus also contains the type of interactions between the different variables that we allow in the model, leading to a system of linear equations:

$$X_t = \boldsymbol{\Theta}\xi. \qquad \text{(Equation 1)}$$

Finally, we apply a regression algorithm to this system, in our case RIDGE regression with sequential thresholding,[55] and generate a family of models for different sets of hyperparameters (regression parameter and the underlying threshold). This approach enforces sparsity in

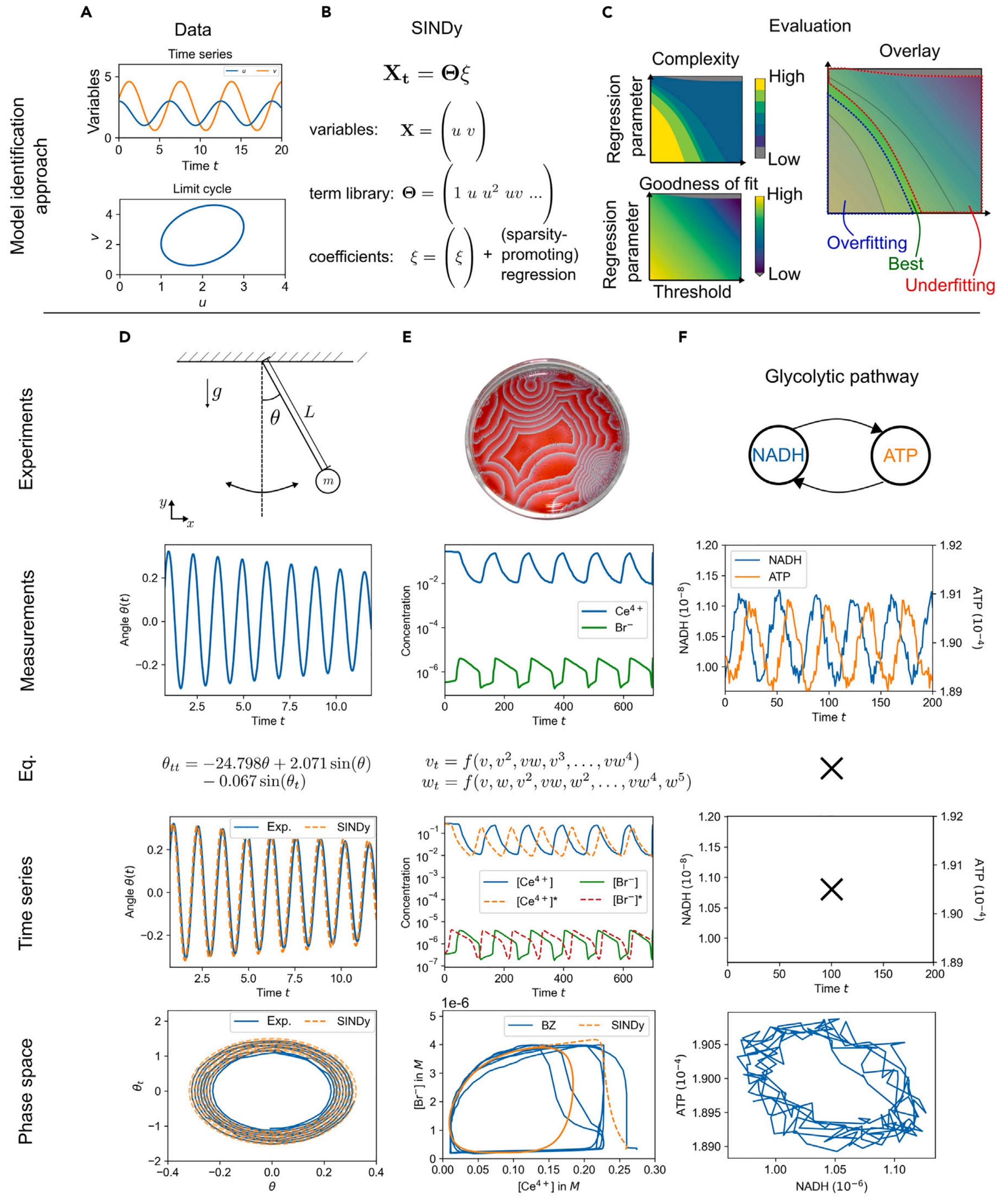

	Simple pendulum	BZ-reaction	Biological oscillator
High resolution	++	+	(-)
Low noise	++	+	--
All variables	++	-	--
Mechanism known	++	++	--

Figure 1. Model identification with SINDy from data of selected, real oscillatory system

(A and B) The SINDy method takes experimental data and creates a system of linear equations with a term library containing all possible terms and their coefficients.

(C) Models are identified by applying a regression algorithm that solves the system. To determine the 'best' model, we scan through the hyperparameters of the regression algorithm and evaluate complexity (the amount of terms selected to be part of a suggested model by SINDy) and goodness of fit (here with the coefficient of determination or R^2 score). By overlaying complexity and goodness of fit we can determine for which sets of hyperparameters the identified models, overfit, underfit or provide the best approximation to the data. In order to identify limitations of the SINDy method, we try to identify models of three selected oscillatory systems from experimental data: The simple pendulum, the Belousov-Zhabotinsky reaction, and oscillations in the glycolytic pathway. The systems and the acquired experimental data represent different levels of data quality, sufficient access to state variables, and knowledge of the underlying mechanisms. This can also be seen by applying the SINDy method to the data: (D) For the simple pendulum, we are able to determine the correct underlying system that reproduces the observed dynamical behavior.

(E) For the BZ reaction, we are able to identify a model that captures the behavior but is not sparse, since it has to account for the nonlinear reduction of the system to only two variables.

(F) Finally, when applied to data from glycolytic oscillations, we see that the SINDy method fails to identify a suitable model. (See STAR methods).

models by cutting off all coefficients ξ and respective terms in the equation which fall below a preset threshold l or are excluded by varying the regression parameter α:

$$\min_{\xi}\frac{1}{2}\|X_t - \Theta\xi\|_2^2 + \alpha\|\xi\|_2 \qquad \text{(Equation 2)}$$

We classify the models by complexity (number of terms involved in the model), which we want to be as small as possible, and a goodness of fit measure, for which we use the coefficient of determination or R^2 score[56] (see Figure 1C). The R^2 score quantifies how well a model is able to explain the observed behavior of the variables, where 1 is fully explanatory and 0 is not. In special cases, the R^2 score can be negative, indicating that the model is not able to account for any dynamical behavior in the data.

We use both complexity and the R^2 score at the same time, as high complexity correlates with high coefficients of determination or over fitting. However, we want to obtain the simplest possible model (low complexity) with the highest possible R^2 score. We determine this by investigating the generated contour plots of complexity and R^2 score (see Figure 1C where we show over-fitted, under-fitted and the 'best' results from visual inspection) and determining the optimal result.

With this simple model identification approach, we set out to identify models from experimental data of oscillatory systems. For this purpose, we choose three different systems with their respective datasets (see Figures 1D–1F): the simple pendulum, for which we acquired the data ourselves from video images; the well-known BZ reaction, for which we use existing data from the original publication by Field, Kórós, and Noyes (FKN)[2]; and time series of glycolytic oscillations between NADH and ATP acquired from Özalp et al.[57]

These three oscillatory systems not only represent three different fields (physics, chemistry, biology/biochemistry), but also differ in their quality in terms of resolution, noise, access to all state variables, and prior knowledge of the underlying mechanisms. The self-generated data of the simple pendulum represents one end of the spectrum, where we have high quality data and the mechanism is known. For the BZ reaction, the data quality is high, but not all state variables are measured. Finally, in the case of most biological oscillatory systems, such as glycolytic oscillations, we lack high quality data, only have information about some of the state variables, and do not have a complete picture of the underlying mechanisms that drive the oscillations.

These aspects are also reflected in the quality of model discovery using SINDy. For the self-generated, high-resolution, and low-noise data of the simple pendulum (see Figure 1D), combined with the knowledge of all variables (term library contains sin and cos, see table in the E-SINDy extension) and the underlying mechanism, the correct form of the ordinary differential equation is easily discovered:

$$\theta_{tt} = -24.798\,\theta + 2.071\,\sin(\theta) - 0.067\,\sin(\theta_t) \qquad \text{(Equation 3)}$$

If we additionally apply the small angle approximation (i.e., $sin(\theta) \approx \theta$,if $\theta \ll 1$) to reformulate the found equation into its well-known form, we see that SINDy provides us with the known equation of a damped simple pendulum. Additionally, we can also derive additional information of the underlying system, such as the length of the pendulum L, the friction parameter b or the mass m (for more details see STAR methods):

$$\xrightarrow{\sin(x)\approx x} \theta_{tt} = -22.727\,\sin(\theta) - 0.067\,\theta_t$$

$$\rightarrow \theta_{tt} = -\frac{g}{L}\sin(\theta) - \frac{b}{m}\theta_t. \qquad \text{(Equation 4)}$$

In the case of the BZ reaction, we have high quality (high resolution, low noise) data, but we only have access to two of the three relevant state variables (see Figure 1E). The BZ reaction, first described by Belousov in 1959 [1], is a family of chemical systems that are an example of non-equilibrium thermodynamics and lead to the emergence of temporal or spatiotemporal oscillations. In their work, FKN studied the bromate-cerium-malonic acid system, where the main interacting compounds are the negatively charged bromine (bromine ions) $[Br^-]$, the positively charged cerium $[Ce^{4+}]/[Ce^{3+}]$, and the neutral bromic acid $[HBrO_2]$[2], which cannot be measured potentiometrically due to its

Table 1. Coefficients of the respective model and the values used in this work

Model	Coefficients ξ
FitzHugh-Nagumo	a, b, c, d, ε $0, 0.5, 1, 1, 0.3$
Goodwin	a, b, c, d, e, f, n, K $1, 1, 1, 0.1, 0.1, 0.1, 10, 1$
Mass action	$k_{p,a}, k_{d,a}, k_{p,g}, k_{diss}, k_{d,g}, k_{pe}, k_{cat}, k_{ass}, k_s, b_{deg}, A_T, P_T, G_T, E_T$ $0.4, 100, 0.05, 1, 20, 6, 4.5, 100, 1.5, 0.1, 1, 1, 1, 3$

neutrality. As a result, this chemical system that has been modeled with the three-component Oregonator model[58,59] must be reduced to two components:

$$\begin{aligned} v_t &= p'(uv + gv - 2fw), \\ w_t &= u - w. \\ \text{with } u(v) &= \frac{(1-v) + \sqrt{(v-1)^2 - 4q}}{2}, \end{aligned} \quad \text{(Equation 5)}$$

with $u = [HBrO_2]$, $v = [Br^-]$ and $w = [Ce^{4+}]/[Ce^{3+}]$. Assuming that we do not have this knowledge about the underlying mechanism, applying SINDy with a term library containing only combinations of v and w will only be able to approximate the reduced system with higher order terms and thus models of high complexity. This results in a quantitatively correct but does not provide us with an interpretable model (see Equation 30 in STAR methods).

For the last case of glycolytic oscillations in yeast, we arrive at the other side of the spectrum, where provided data from Özalp et al.[57] is scarcely sampled and has high noise levels (see Figure 1F, for more details see STAR methods). Glycolysis has been intensely studied over the last 70 years[60,61] and is a process that takes place in prokaryotic and eukaryotic cells in order to convert glucose to smaller substances. The main function is to provide the cell with adenosine triphosphate (ATP) when respiration does not take place.[62] If dense suspensions of non-growing cells or cell-free extracts of the yeast *Saccharomyces cerevisiae* are starved, temporal oscillations can appear.[61] The main driver behind glycolytic oscillations are dynamics of adenosine diphosphate (ADP) and ATP interactions,[63] which form the basis of the most prominent model of glycolytic oscillations, the Selkov model[64]:

$$\begin{aligned} u_t &= au\,(uv - 1), \\ v_t &= 1 - u^2 v, \end{aligned} \quad \text{(Equation 6)}$$

with the dimensionless $u = [ADP]$ and $v = [ATP]$.

Glycolytic oscillations are usually measured through the autofluorescence of the hydrogenated nicotinamide adenine dinucleotide (NADH) which oscillates in phase with ADP,[65] as most chemical compounds taking part in glycolysis are optically silent.[62] The dataset we use, measures the oscillations of NADH, or indirectly of ADP and intracellular oscillations of ATP.[57] However, SINDy is not able to identify suitable models in the form of the Selkov model (nor any other form) from the provided experimental data.

Challenges of model inference

From this naive application of the SINDy method on experimental data, we identify four main challenges found in (biological) oscillatory systems:

Insufficient resolution: Sufficient resolution plays a crucial role in model identification in general and for SINDy in particular; SINDy reportedly struggles in low-data scenarios[50,66,67], which has led to proposals to extend the method.[49,68,69] However, the limitations of SINDy and the proposed extensions have not been sufficiently studied, and their proof of concept has been done on generic examples, such as the Lorenz system. Such systems usually do not reflect the dynamical behavior of real biological oscillators, which are often characterized by alternating slow and fast dynamics,[12] resulting in pulse-like interactions of successive long/slow and short/fast phases called timescale separation, which can be difficult to capture if the resolution is insufficient. Alternative sampling approaches have been proposed here,[70] but optimizing sampling strategies requires prior knowledge of the dynamics or may be impossible due to technical limitations.

High noise: Besides low-data limits, SINDy has also shown reduced performance when the data are noisy,[42,66] since SINDy fits the derivative $\boldsymbol{X}_t$ and not the actual measured time series, which can lead to non-unique solutions.[71] Several ways of dealing with this have been proposed,[49,69,72] and Delahunt and Kutz have developed a toolkit for noise handling when applying the SINDy algorithm.[73] For the special case of biological transport models Lagergren, Nardini et al.[74,75] have shown that using additional noise filtering via a neural network on (spatio)temporal data can significantly improve model identification with regression algorithms. However, the toolkit and other extensions also provide a proof of concept in dynamical systems that do not represent biological oscillatory behavior or experimental data, i.e., strong timescale separation and/or insufficient temporal resolution. Thus, the limits of the methods in experimental situations are not fully known yet, and several extensions suggest the application of additional noise filtering[69,73] without evaluating the impact of this choice on model identification.

Number of dimensions: In order to derive correct models from data, SINDy needs information about all relevant state variables (also called dimensions) that are able to fully describe the dynamical systems. By 'relevant state variables', we refer to the smallest, finite

Table 2. Best discovered equations ($R^2 > 0.9$ from Figure 6B) with data from the Goodwin oscillator in Equation 8 with no noise and 398 ppp using the SINDy-PI method with a library only containing terms already known from the model

	Equations
Ground Truth	$u_t = -0.1u + \frac{1.0}{1.0+w^{10}};\ v_t = u - 0.1v;\ w_t = v - 0.1w$
Candidate model 1	$u_t = -0.1u + \frac{0.03}{w^9} + \frac{1.0}{w^{10}};\ v_t = u - 0.1v;\ w_t = -\frac{67.0v}{19.0w - 100.0} + \frac{6.0w}{19.0w - 100.0}$
Candidate model 2	$u_t = -0.11u + \frac{0.03}{w^9} + \frac{1.0}{w^{10}};\ v_t = u - 0.1v;\ w_t = \frac{50.0v}{17.0w+21.0} - \frac{5.0w}{17.0w+21.0} + \frac{0.5}{17.0w+21.0}$
Candidate model 3	$u_t = -0.11u + \frac{0.03}{w^9} + \frac{1.0}{w^{10}};\ v_t = u - 0.1v;\ w_t = \frac{50.0v}{17.0w+21.0} - \frac{5.0w}{17.0w+21.0} + \frac{0.5}{17.0w+21.0}$

number of variables needed for an unambiguous description of a dynamical system.[76] Often such knowledge is not provided and either too many or not enough variables describing a system are measured, an example being the BZ reaction where one dimension is missing. Again, several extensions have been proposed that involve the use of auto-encoders[77,78] or delay embedding[70,79] to reconstruct dimensions or reduce the system. However, these approaches require high quality data to provide sufficient information to unfold missing dimensions or reduce existing ones, and therefore do not reflect data on dynamical systems in biology, where sometimes a variety of dimensions (e.g., fluorescent markers) are measured but suitable temporal data are lacking. Furthermore, in the case of high-dimensional systems we also encounter the so-called 'curse of dimensionality',[80] which obstructs the derivation of relevant information from such systems. Especially for biological oscillatory systems, this can pose significant challenges for parameter estimation, either with SINDy or other methods.[81]

Limited prior knowledge: Some of the above challenges can be overcome if there is prior knowledge about the underlying system. Such knowledge can be respecting basic physical laws, e.g., conservation of mass, or the implementation of already known interactions between certain actors of a system. When such information is available it is more likely that data-driven model identification will be able to identify physically sound, interpretable models, but in many situations in biology, knowledge beyond basic physical laws is not available.

These challenges are always at least partially present in any experimental domain, but especially for experimental biological systems they can pose challenges for model identification. In systems such as the simple pendulum, which is a 'simple' example with high-resolution, low-noise experimental data and a substantial amount of prior knowledge, identification is easy: we know that we have to obtain the angle θ to identify the underlying model. However, for more realistic systems it becomes increasingly difficult (BZ reaction), if not impossible (glycolytic oscillations). Therefore, we aim to characterize the influence of low-data limits and noise when evaluating biological oscillatory systems with SINDy and to answer the following questions.

Q1. *What are the general limitations for the identification of (biological) oscillator models with respect to data availability, resolution, and noise?*
Q2. *How does the choice of common noise filtering techniques affect the success of model inference for oscillatory systems?*
Q3. *What is the role of strong time-scale separation in biological processes in model recovery?*
Q4. *How do different nonlinearities in the formulation of biological oscillator models affect model inference?*
Q5. *How can model identification for high-dimensional oscillator systems work in low-data limits?*

While answering the questions, we aim to address challenges faced by many experimentalists wanting to apply this method on their experimental data and provide a broad overview of relevant aspects that have to be taken into account when doing so.

Impact of data and code availability, sampling, and noise on model inference from synthetic data

We begin our investigation by examining the availability of data (the amount of information provided in a time series), the sampling of data, and the influence and mitigation of noise. To address these questions and the other questions, we start with synthetic data generated from a set of generic, biologically motivated oscillator models that represent a non-exhaustive variety of model architectures in biology.

Generating synthetic datasets

Mathematical models used in biology can generally be classified by their dimension, or set of state variables, and the complexity of the interactions they describe, which in this case is the order of the terms included in the mathematical model (see Figure 2). Thus, models in the model space of possible descriptions of a system can be seen as closer to biological reality if they use only simple lower order interactions obeying mass action kinetics and provide complex dynamical behavior through more dimensions. In contrast, models that take a higher-level approach and abstract high-dimensional systems with more complex interactions are a conceptual representation of biological reality. Both modeling principles have advantages: biological models allow us to directly relate certain behaviors to biological actors, but conceptual models allow us to more easily study the dynamical behavior of a system. Models that lie outside the model space are either overly complicated or overly simplified, and thus provide insufficient or redundant information.

From this defined model space, we select three models that cover specific aspects and have been used to describe different biological systems.

FitzHugh-Nagumo. The FitzHugh-Nagumo (FHN) oscillator was developed in the 1960s to describe the oscillatory spiking of neurons,[17] but can also be used as a high-level description of other biological systems, such as cardiac dynamics,[82] and early embryonic cell cycle oscillations.[83] This model has a moderate complexity in its interactions between the variables, using a cubic nonlinearity instead of typical mass action dynamics. However, the FHN model allows oscillatory behavior in only two dimensions. We used the FHN equation of the following form:

$$\begin{aligned} u_t &= -u^3 + cu^2 + du - v, \\ v_t &= \varepsilon(u - bv + a), \end{aligned} \quad \text{(Equation 7)}$$

where ε is varied in the later stages (other coefficients are shown in Table 1). Here, the variables u, v correspond to a membrane potential and potassium and sodium channel reactivation (for neurons), excitation and recovery of cardiac cells (cardiac dynamics) or activity of the APC/C complex that inhibits the activity of Cyclin B-Cdk1 complex by degradation of Cyclin B, which is pushing a cell into mitosis (early embryonic cell cycle).

Goodwin. The Goodwin (G) oscillator was developed by B. Goodwin, also in the 1960s, in order to describe the phosphorylation/dephosphorylation processes of a transcription factor[19,20] or circadian rhythms.[20] This model has been widely extended and studied over decades and has a higher complexity of nonlinear interactions than the FHN oscillator through the nonlinear response curve in the form of a Hill function $H(x)$, while avoiding any other higher order interactions between the variables. The delay of the negative feedback is implemented by an additional variable. Here, we use the Goodwin oscillator in the following form,

$$\begin{aligned} u_t &= aH(w) - du, \\ v_t &= bu - ev, \\ w_t &= cv - fw \end{aligned} \quad \text{(Equation 8)}$$

with the Hill-function defined in function of an arbitrary variable x as:

$$H(x) = \frac{K^n}{K^n + x^n}. \quad \text{(Equation 9)}$$

The coefficients can be found in Table 1. The variables u, v, w can be, e.g., interpreted as a clock-mRNA, clock-protein, and a repressor (circadian rhythm).

Mass action. Mass action models are used to describe the dynamics of a wide variety of biological systems. They are characterized by more variables (higher dimensional), but simpler, mostly low-order interactions as their rate of change is directly proportional to the product of their activities or concentrations.[84] Such interactions typically consist of linear or quadratic terms. In this work we use the cell cycle mass action model developed by Hopkins et al.,[85] which describes the oscillations of the early embryonic cell cycle of *Xenopus laevis*, based on low-order (mass action type) interactions of six interacting molecules, avoiding complex descriptions of interactions in the form of ultrasensitive response curves or higher order terms.[86] The model equations are as follows:

$$\begin{aligned} u_t &= k_{p,a}(A_T - u)v - k_{d,a}u(P_T - y), \\ v_t &= k_s - b_{deg}uv, \\ w_t &= k_{p,g}(G_T - w)v - k_{d,g}(P_T - y)w, \\ x_t &= -k_{pe}xw + k_{cat}y, \\ y_t &= k_{ass}(E_T - x - y)(P_T - y) - k_{diss}y - k_{cat}y. \end{aligned} \quad \text{(Equation 10)}$$

for which the parameters can be found in Table 1. Here, similarly to the FHN model for the cell cycle, the variables of u and v are interpreted as CyclinB-Cdk1 and APC/C activity.

In order to study model identification in experiment-like circumstances, we simulate one single time series of the respective models with a time step of $dt = 10^{-3}$. We control the amount of information by changing the number of periods T included in the simulated time series $t_{\text{sim}} = n_{\text{periods}}T$ (see Figure 3A). Using a fixed number of periods in the time series allows us to compare the results of different oscillatory systems despite their different period lengths. We further impose low-data limits by subsampling the simulated time series equidistantly to mimic typical experimental situations. To further resemble experimental situations, we add random (white) noise η which is normally distributed (Gaussian noise) to the simulated datasets consisting of fractions of up to 10% of the standard deviation σ of the signal itself (In Halley et al.[87] the authors describe measurement noise in ecology and other biological processes to be pink or 1/f noise which has a linear frequency spectrum on the logarithmic scale; however, both noise colors can be distributed normally and the choice of noise color should not impact model identification).

$$\begin{aligned} \eta_i &= \beta\sigma X_i \quad \beta = 0, \ldots, 0.1 \text{ with } \Delta\beta = 0.01. \\ \rightarrow \tilde{X}_i &= X_i + \eta_i \end{aligned} \quad \text{(Equation 11)}$$

It should be noted, that when scanning over the hyperparameters and using only a single time series can lead to varying model recover success (for a smaller threshold l identification is possible while for a slightly larger not) due to the variable nature of regression and the use of a random seed to generate the normally distributed noise. However, in Figure S1 we show that despite this variability the overall outcome of our investigation is independent from the choice of seed.

Length of time series, equidistant sampling, and added noise

The evaluation of the length of the time series is important for the correct choice of experimental measurements, but also for the rest of the following study, since we choose the length of the time series to evaluate the performance of SINDy.

To do this, we simulate sets of time series for all models, varying the number of periods included: $n_{\text{periods}} = 1 \ldots 10$. At the same time, we vary the number of points per oscillation period and determine the minimum sampling rate required to successfully identify the underlying dynamics (see Figure 3B). We see that the required number of points per period (ppp) increases with the number of dimensions: The two-component FHN model requires at least 95 ppp, while the Goodwin and mass action models require 200 ppp (3 components) and 4500 ppp (5 components), respectively.

Furthermore, we see that the amount of ppp is reduced as more periods than one are included, but when the dataset contains more then 2 periods increasing the number of periods involved does not influence the performance of SINDy. However, to avoid any potential influence on oscillations with strong timescale separation from the low number of periods, we decided to evaluate the performance of SINDy on time series of length $t_{\text{eval}} = 4T$.

In the following section we focus on data and noise bounds rather than dimensionality, we apply SINDy to synthetic data from the two-dimensional FHN model (Equation 7). We define a successful identification, when SINDy selects all correct terms from the term library and identified coefficients lie within 2% of the true coefficients (marked in yellow, see Figures 3C–3F). If the coefficients lie beyond this threshold, SINDy was sometimes still able to recover the correct form of the underlying equation, thus providing important information on the system's dynamics (marked in turquoise, see Figures 3C–3F). Otherwise, when model recovery was entirely unsuccessful, we colored this in dark blue (see Figures 3C–3F).

We start by applying SINDy to equidistantly sampled data from the FHN model, where we add different levels of Gaussian noise up to 10%. SINDy is able to correctly identify the underlying dynamics when there are at least 42 ppp and the added noise levels are low (below 2%, see Figure 3C). This high sensitivity of SINDy to noise has already been reported in the literature.[42,49,72,73,88–90] To handle such noise and improve performance, different noise filtering techniques were proposed,[72] and more advanced methods were developed,[49,89,90] which we will consider later.

Noise filtering techniques

Recently, in Cortiella et al.,[91] an extensive analysis on the impact of selected noise filtering approaches for accurate model identification with SINDy has been conducted. Here, we partially extend this analysis by specifically focusing on model recovery in biologically motivated oscillatory systems. We select four different, commonly applied filtering techniques: A simple low-pass filter, a Wiener filter, a nonlinear filter based on local phase space averaging (LPSA)[92] and the Savitzky-Golay filter proposed in Lejarza et al.[72]

Low-pass filter: The low-pass filter is a frequency filter that reduces the amplitude of high frequencies in a signal, which in the case of time series are the fast fluctuations of noise.

Wiener filter: The Wiener filter is an enhanced low-pass filter, which assumes that noise is of high frequency and normal-distributed, which is the case for our added noise.

LPSA: The local phase space averaging is a simple nonlinear filter, which averages the variability of measured variables in the phase space.

Savitzky-Golay filter: The Savitzky-Golay filter regresses a low-order polynomial (e.g., third order) within a changing selected subset of data (moving window) in order to approximate the local changes while preserving the global trend.

The application of these methods generally leads to an improved model identification for the FHN model (see Figure 3D).

In particular, the low-pass filter was able to provide successful identification for high noise regimes because it is able to separate the normally distributed noise from the actual signal. However, for low-data and lower noise levels, the low-pass filter was not able to identify the model. This is a result of an imprecise cutoff frequency, which allows noise frequencies to be present in the time series. Selecting this cutoff frequency can be particularly difficult in low-data limits, as it can affect the shape of the oscillations and thus prevent correct model identification.

The Wiener filter consistently identifies the correct form of the underlying FHN model despite high noise levels when sufficient data is available (>280 ppp). However, the recovery fails when less data is available, due to the Wiener filter's fundamental assumption that the noise must be normally distributed: As the amount of data decreases, the identified error is no longer normally distributed, but uniform (we provide a detailed overview of the performance of noise filtering in STAR methods, see Figure S4).

The LPSA method is able to correctly identify the FHN model with the same number of points per period as the original SINDy and the low-pass filter. However, compared to the low-pass filter, it performs better in low-noise situations, while inconsistently identifying the dynamics at higher noise levels. As we show in the STAR methods, we see that this method is strongly dependent on the correct choice of delay in the approximation and is thus not able to filter stronger variability in high noise situations.

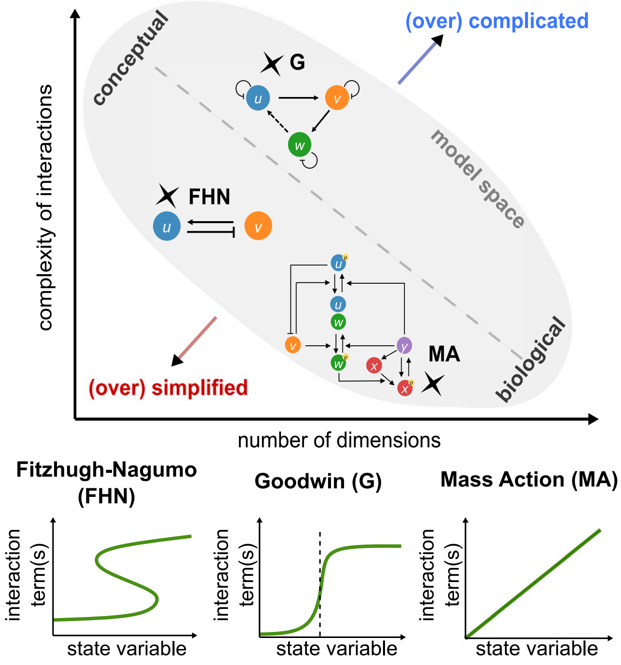

Figure 2. Classification of oscillator models in the model space of biological processes

Biological (oscillator) models can be characterized under two aspects: complexity of interactions and number of dimensions (state variables). There is a model space where both aspects are leading to functional models. If a model has low complexity of interactions and low number of dimensions, it is usually (over) simplified, or if both aspects are high it is (over) complicated. Models on the diagonal provide a trade-off between both aspects. In our work we consider three generic biological (oscillatory) models that can be applied to a range of biological systems: FitzHugh-Nagumo oscillator (with cubic (bistable) interactions), Goodwin oscillator (ultrasensitivity in the form of a Hill function) and the (cell cycle) mass action model (with lower order interactions).

Finally, we studied the Savitzky-Golay filter, which was proposed by Lejarza et al.[72] to improve SINDy by applying a moving horizon (or window) optimization approach. We find that the Savitzky-Golay filter works well, but requires more data than low-pass filtering or LPSA, i.e., at least 100 ppp. For higher noise levels (above 6%) using the Savitzky-Golay filter does not allow SINDy to correctly identify the underlying system. This is due to the low order polynomial approximation (regression) in moving windows: The higher the variability, the more precise must be the window size on which the regression is applied. Otherwise, the regression will overestimate the variability of the signal, resulting in a locally incorrect representation of the signal.

In conclusion, by choosing an appropriate (or wrong) filtering technique for the specific noise and data properties of the signal one can significantly improve (or hinder) model identification with SINDy. Even though all noise filtering techniques studied are capable of improving system identification, either too strong or too weak noise filtering can hamper data-driven discovery, as it can alter the shape of the oscillatory signal. This is especially important for biological oscillations that can contain multiple time scales, such as pulse-like behavior. Changing the shape of such pulses can then lead to a false description of the system.

Different time scales in the system

Whenever a dynamical system is characterized by multiple time scales, this has general implications for regression-based model identification techniques such as SINDy. Timescale separation can be easily controlled in the FHN model by varying the parameter ε: for small $\varepsilon \ll 1$ the dynamics of *u* and *v* are strongly separated in time, resulting in relaxation (pulse-like) oscillations, while for large $\varepsilon \approx 1$ the dynamics are no longer separated and the oscillations become sinusoidal (see Figure 3E).

In an equidistant sampling scenario, the strength of the timescale separation plays an important role for a successful model identification, as can be seen in Figure 3E. Here, we see our previously obtained results from Figure 3B with the FHN and $\varepsilon = 0.3$. If we increase $\varepsilon = 1$, SINDy can identify the correct model equation for a smaller number of points (>15 ppp) and even in some cases for all tested noise levels (up to 10%). However, decreasing ε increases the amount of data required ($\varepsilon = 0.3 - 42$ ppp, $\varepsilon = 0.1 - 116$ ppp). and in the case of $\varepsilon = 0.01$ we are not able to recover the model with the provided amount of data (500 ppp). If the fast changes are not sufficiently sampled, the solutions will contain more spurious terms, despite the use of sparsity-promoting optimization algorithms.

In this context, we also examine how noise filtering can change the identification success in the presence of timescale separation. We only evaluate the success with the FHN model and $\varepsilon = 0.1$ (see Figure 3F). Here, by applying a low-pass or Wiener filter, SINDy fails to identify a correct model in the presence of noise. This is again a consequence of the precise choice of cutoff frequencies, which can lead to the removal of high frequencies associated with the fast pulses, thus underestimating the strength of the timescale separation.

In this case, both the nonlinear LPSA method and the Savitzky-Golay filter are able to provide better results, although only for larger amounts of data (LPSA - about 200 ppp, Savitzky-Golay - about 230 ppp). The LPSA is able to handle lower levels of noise because it does not approximate the time series globally over time, but locally in phase space. With a sufficient number of points in time intervals of fast changes (horizontal and vertical edges of the limit cycle in phase space) and transitions to these phases (corners of the limit cycle in phase space, see Figure 3E), the technique is able to capture the different time scales correctly. In the case of a Savitzky-Golay filter, the changes can be captured because again the fast dynamics of the oscillations are approximated locally within the moving window. Thus, with a sufficient temporal resolution, identification can be successful.

Addressing noise and low-data in equidistant sampling with multiple trajectories

We see that identification of symbolic models of oscillatory systems is difficult when the data itself and its quality are modified to resemble experimental situations, even when we apply noise reduction techniques. Another suggested way to mitigate the problems of both low-data and high noise is to provide more than a single time series or trajectory.

Recently, two possible approaches have been proposed: The Ensemble-SINDy or E-SINDy extension,[49] which applies bootstrapping, or more specifically bagging, to data and/or term library, thus synthetically increasing the amount of data that can be used to infer the underlying dynamics (for more details see STAR methods), and providing more trajectories, which has been shown to increase the success of model recovery.[89,90] Both approaches are conceptually similar in that they try to feed SINDy with more data from different situations, thus limiting the possible model space to models that can account for different trajectories.

We apply both approaches to data from the FHN model with $\varepsilon = 0.3$ in Figure 4. It can be observed in Figure 4A that E-SINDy performs worse than SINDy on the data provided, this in contrast to the results in Fasel et al.[49] For smaller amounts of noise, E-SINDy is not able to identify the underlying model, which in this case means that not all relevant terms appear in 90% of all submodels from the bootstrapped data (also called the inclusion probability p_{inc}, which has to be larger than our chosen threshold probability $p_{\text{thres}} = 0.9$). We use this relatively high threshold compared to the original publication because in the case of unknown underlying model we are not able to choose an appropriate p_{thres} *a-priori*.

To understand the reduced performance, we examine the dependence of the inclusion probabilities on the amount of data and the noise level (see Figure 4B). We see that without noise $\eta = 0$, E-SINDy needs at least 50 ppp to not only correctly select the terms, but also to reduce the amount of mostly mixed terms included in the inferred model of u_t. Furthermore, the identification of the correct term breaks down when noise is included in the time series. Even at low noise levels, p_{inc} of the v term in v_t rapidly falls below the assigned p_{thres}, while at high noise levels a wide range of non-relevant terms are included in the model. This begs the question why we are not able to achieve similar results as shown in Fasel et al.[49] The answer lies in the bagging method itself and the choice of data used in the original publication: Bagging,[93] which stands for bootstrap aggregation, is a method that improves the predictive power of e.g., regression algorithms. However, bagging is a smoothing operation that reduces the variance of the signal,[94] which means that aspects such as timescale separation in limits of low-data and/or high-noise may be incorrectly smoothed and thus incorrectly approximated by SINDy. Indeed, in Fasel et al.,[49] the signals either do not contain multiple time scales when studying a low-data limit, or large amounts of data are used if the variance is high. Thus, applying the E-SINDy method to the special case of biological oscillations may lead to unsatisfactory results due to bagging.

In contrast, increasing the number of trajectories available to SINDy without smoothing by bagging, as suggested by Ermolaev et al.,[89] can allow to preserve the slow-fast changes in the oscillations. Indeed, we see that by introducing more trajectories of the same system with randomly chosen initial conditions (IC), we are able to significantly improve the performance of SINDy (see Figure 4C). With two included time series, the minimum number of points is reduced to about 25 ppp, but the noise handling does not improve. If more trajectories are included (more than 8, Figure 4C shows only a subset of the results), the required amount of data increases to 55 ppp, but SINDy is able to tolerate all introduced noise levels and can provide the correct form of the underlying model. The increased number of points is due to the variability introduced by multiple trajectories in low-data limits, which hinders the identification of the correct equation and simultaneously reduces the coefficient values when more data are available.

To address this issue, the models, identified with multiple trajectories, can be used as the basis for an adjacent simple parameter approximation where only the parameters of the identified model are optimized. This application leads to the correct identification of coefficients for low noise levels and reduced coefficients for high noise levels, thus improving the performance of SINDy for low noise levels (see Figure 4D). With this we are able to improve the performance of SINDy without any additional noise reduction technique nor an increase in the sampling of the corresponding time series of experiments.

However, such an approach does not show improved performance for stronger timescale separation than $\varepsilon = 0.3$. We have also obtained the results for the FHN with $\varepsilon = 0.1$, which can be found in STAR methods, and despite the slightly improved handling of up to 6% additional noise, the number of points required is 2.5–8 times higher than for $\varepsilon = 0.3$ or when only SINDy is applied (see Figure 3E).

Mitigating timescale separation with improved sampling strategies

Another possibility suggested in Champion et al.[70] is the use of other sampling strategies, such as burst or specifically optimized sampling.

Therefore, we set out to evaluate whether optimizing sampling strategies is able to improve model identification in the presence of strong timescale separation. Here, we apply a different sampling approach that requires more knowledge about the underlying system than burst sampling, but should be able to provide more information about the dynamics: We keep the total number of points per period constant, but vary the distribution of points in the slow δ_s or fast δ_f changes of the time series, so that $1 = \delta_s + \delta_f = (\delta_{s1} + \delta_{s2}) + (\delta_{f1} + \delta_{f2})$ (see Figure 5A). The

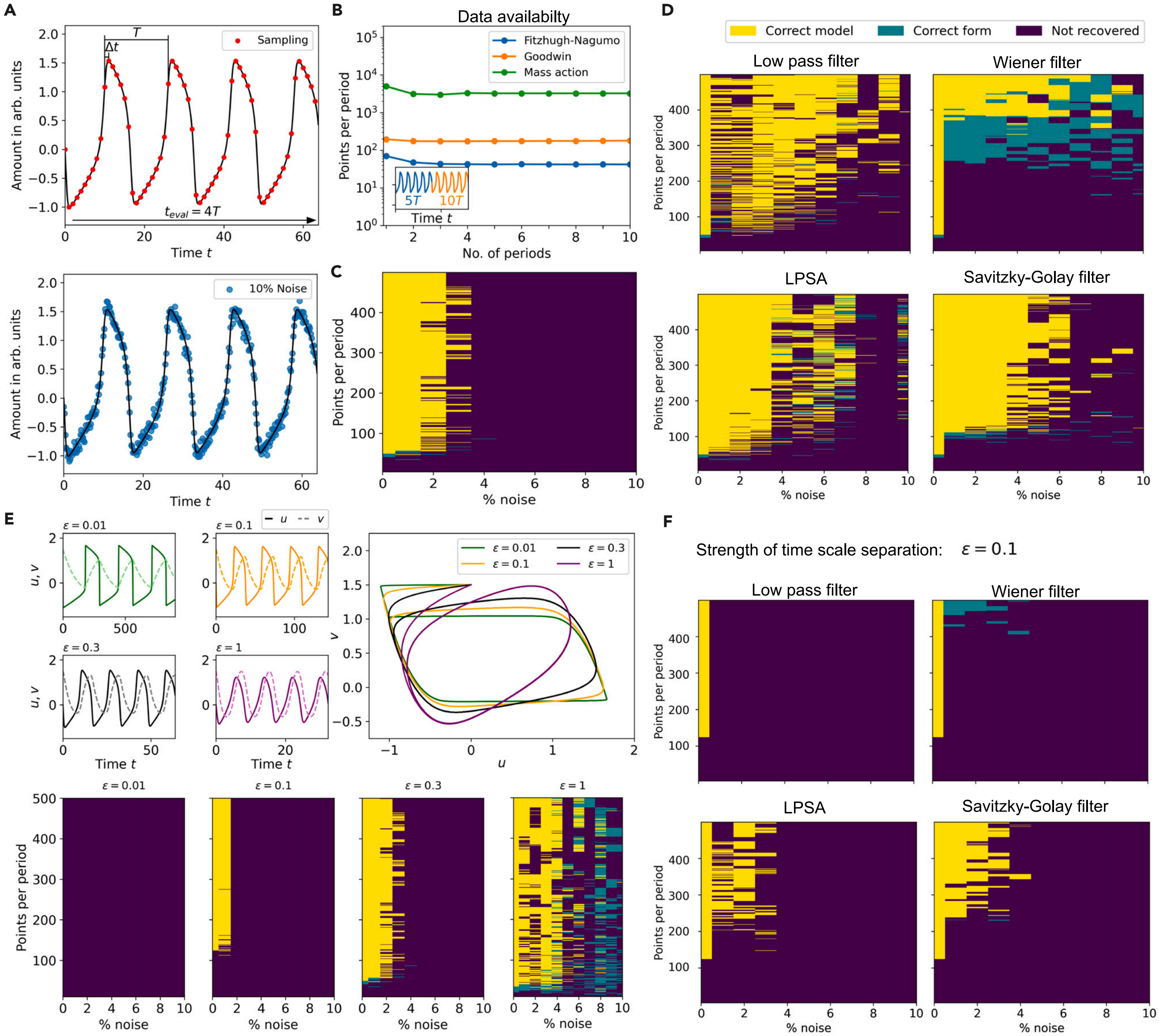

Figure 3. Investigation of data availability, equidistant sampling and added Gaussian noise for weak and strong timescale separation ε in the FHN model

(A) The chosen models are simulated to generate one time series with $dt = 1 \cdot 10^{-3}$ which are later subsampled to simulate low-data limits. Noise is added in the form of up to 10% Gaussian noise.

(B) By varying the length of the time series by the information content in information units (periods), we determine that increasing the length of the time series does not affect the amount of points needed for model recovery if at least 4 periods are present.

(C) Combining simulated time series of length $t_{\text{eval}} = 4T$ and added Gaussian noise, SINDy is able to recover the underlying model correctly (yellow) or its correct form (turquoise) for at least 45 points per period with up to 3% noise.

(D) Noise reduction techniques (low-pass filter, Wiener filter, LPSA and Savitzky-Golay filter) are able to improve the performance of SINDy for higher noise levels, however, the success depends on underlying methodology (more details in text).

(E) An important aspects of biological oscillatory systems is timescale separation, which can be changes with the ε parameter in the FHN model. For stronger timescale separation (small ε) identification requires high-resolution/low-noise data and fails for to strong separation.

(F) The strength of separation also influences the performance of SINDy with noise filtering, where frequency filters (low-pass and Wiener filter) fail and techniques which estimate noise locally (LPSA and Savitzky-Golay) are superior.

part of the time series assigned to fast changes is $\alpha_1 + \alpha_2 = 0.2T$, or 20% of the time period T, so if $\delta_s = 0.8, \delta_f = 0.2$ we get equidistant sampling. For a timescale separation of $\varepsilon = 0.3$, already increasing the number of points in fast changes improves the performance, with an optimal point at a 50/50 distribution (see Figure 5B).

The performance improvement is only successful for low noise levels (as shown in Figure 5B), because computing derivatives in fast changes with small steps introduces more error due to increased variability, thus reducing performance.

However, for low noise levels, this method improves successful model recovery for even stronger timescale separation of $\varepsilon = 0.1$ (see Figure 5C). By increasing the fraction of points δ_f, we are able to reduce the minimum number of points required from 115 ppp with equidistant sampling to 40 ppp.

Summary of the impact of data quality aspects on model identification (answers to Q1, Q2 and Q3)

In the first part of the study, our goal was to answer what the sampling and noise limitations of SINDy are, and how do these limitations interact with the specific feature of timescale separation in biologically motivated oscillatory systems.

We find that successful recovery of the underlying models of oscillatory behavior depends more on the number of dimensions than on the number of periods provided in the time series. This has direct implications for experimental investigations, suggesting that high-frequency measurements should be preferred over long measurement times. Furthermore, we have shown that sufficient sampling is a key feature to recover underlying mechanisms and, as in most model identification, the more temporal data the better. However, more temporal data may not provide better performance when faced with high noise levels and/or strong timescale separation in the signal of oscillations (Q1). For the first part, we show that the introduction of noise filtering techniques can indeed provide a significant improvement in performance, but in low-data situations it can hinder identification if not set up precisely. In addition, when considering strong timescale separation, noise filtering can significantly reduce the success of the investigation and can only provide improvement when large datasets are provided. Thus, even if data cleaning from experiments is able to provide a visually good signal, it may introduce artifacts that prevent identification of the underlying dynamics (Q2).

We have tried to avoid these aspects by studying the E-SINDy method and introducing more time series trajectories. Here, we see that it is possible to avoid the application of noise reduction techniques and increasing sampling rates when there is a large number of trajectories. However, we show that the E-SINDy application, although undoubtedly applicable to low-data and high noise situations, is not suitable for relaxation oscillation data, since the applied bagging smooths the measured signal and acts as an unwanted signal filtering.

To enable identification for smaller timescale separations, we investigated whether an optimized sampling strategy could improve SINDy's performance. Indeed, we were able to reduce the number of points to one-third even for $\varepsilon = 0.1$ when equidistant sampling is applied. However, locally increased sampling, besides requiring prior knowledge about the system, only increases successful recovery when noise levels are low, since variability introduced in the derivatives on which SINDy regresses hinders correct identification of fast changes.

In general, the realistic case of strong timescale separation in experimental oscillatory data (high noise) is the most relevant limiting aspect when applying SINDy. Even if large amounts of data are available, identification can become either difficult or impossible (Q3), which makes SINDy (or the extensions studied here) applicable only to near-sinusoidal oscillatory systems, with important implications for its use in the field of systems biology.

Influence of higher-order nonlinearities and high system dimensionality on model inference

After investigating the importance of data quality when using SINDy, we now turn to another important aspect of biological oscillatory systems: balancing the dimensionality of the model (number of components) and the complexity of the interactions between those components (see Figure 2). While more complex higher-order nonlinear interactions can reduce the number of required state variables (lower model dimensionality), using many more components (higher model dimensionality) allows to use simpler low-order mass action interaction dynamics.

Ultrasensitivity in the Goodwin oscillator

In the FHN which we have used to study the data availability aspects, the nonlinearities are introduced in the form of a cubic polynomial that allows us to be recovered using standard SINDy. However, some biologically motivated oscillator models, e.g., the Goodwin model, chose to introduce nonlinearities in the form of ultrasensitive response curves that can be described by the Hill function shown in Equation 9. For a three-dimensional system (three interacting components) it has been shown that the required power of nonlinearity has to be at least 8: $n \geq 8$.[95]

The standard SINDy method is not able to identify the Hill function or any other rational function from data, except if it can be approximated by higher order terms (as we could see in the case of the BZ reaction see Figures 1 and S3) or if the functional form of the nonlinearity is provided. From Figure 6A we see that if we generate time series with oscillatory behavior ($n = 10$), SINDy is able to approximate the behavior, but provides uninterpretable expansions of the Hill function (see STAR methods) of the respective order. To address this problem multiple extensions have been provided during the last years, most notably the SINDy-PI (parallel implicit) which reformulates an equation with rational terms into an implicit form[96]:

$$\begin{aligned} \text{SINDy} : X_t &= f(X, \xi), \\ \text{SINDy} - \text{PI} : X_t &= f(X, X_t, \xi). \end{aligned} \qquad \text{(Equation 12)}$$

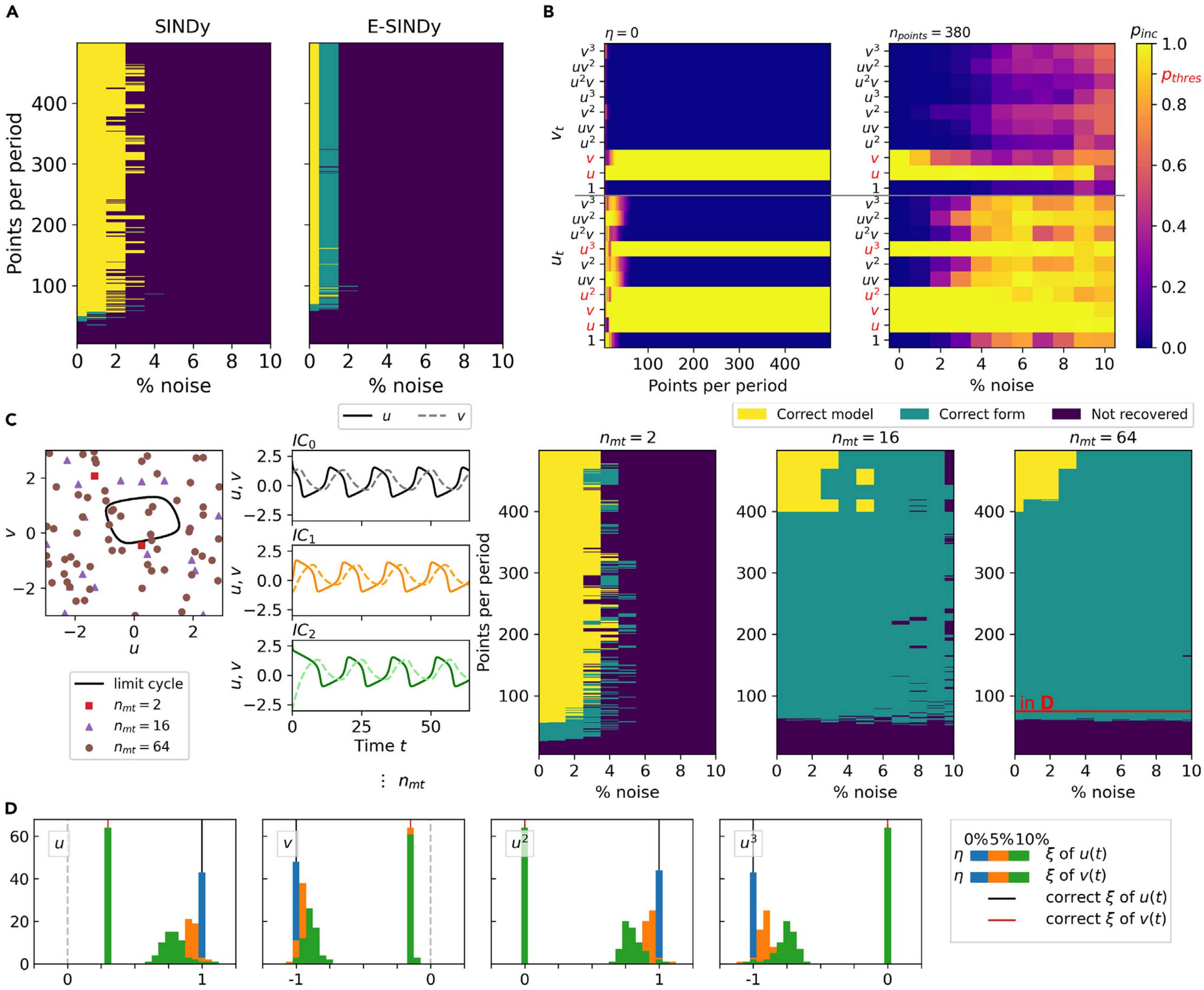

Figure 4. Addressing low-data and high noise with multiple trajectories

(A) Despite the claims of,[49] the application of E-SINDy (right) compared to just SINDy (left) does not improve model recovery.

(B) Inspection of the respective term probabilities to be included p_{inc} in the inferred model (threshold for inclusion in equation is $p_{\text{thres}} = 0.9$), show that E-SINDy underestimates the probability of several terms (e.g., v for v_t) and overestimates mixed terms (e.g., uv for u_t).

(C) Providing more trajectories of the underlying dynamics with different, random initial conditions (IC) leads to an improved identification of the correct form of the FHN equation. The different IC are shown in the left panel: squares for two ICs, triangles for 16 ICs and circles for 64 ICs.

(D) Applying a subsequent nonlinear regression algorithm on noisy and sparse data with the identified models allows to identify the correct coefficients.

Thus, the rational form of possible models is translated into a pure polynomial form and becomes solvable with the original SINDy approach. For the Goodwin model in Equation 8, the first equation for u_t can be transformed into the following target for SINDy-PI (with $K = 1$ and a deliberately chosen n):

$$u_t = a - du - duw^n - u_t w^n, \qquad \text{(Equation 13)}$$

and by including the derivative u_t in the model identification process, the rational terms can be identified. However, the suggested SINDy-PI extension in Kaheman et al.[96] has only been shown to provide satisfying results when tested on synthetic data with more then 900 trajectories. As we have shown in the previous section, including more trajectories can indeed improve the identification notably. However, such large amounts of high-quality data are often not available in experimental setups, which has led e.g., Brummer et al.[53] to reject the use of SINDy-PI in their work.

Nevertheless, the SINDy-PI extension provides the unique possibility to identify rational terms in a model within a sparsity promoting regression framework and we want investigate if SINDy-PI is able to discover either the underlying model or at least provide information on the rational nonlinearities in the Goodwin model. The original SINDy-PI uses STLSQ to promote sparsity; here, we use the SR3 regression with ℓ_1 regularization instead which is close to LASSO regression[97]:

$$\min_{\xi, \boldsymbol{w}} \frac{1}{2} \| \boldsymbol{X}_t - \boldsymbol{\Theta}\xi \|_2^2 + \alpha \| \boldsymbol{w} \|_1 + \frac{\kappa}{2} \| \xi - \boldsymbol{w} \|_2^2 \text{ with } \alpha = \frac{l^2}{2\kappa} \qquad \text{(Equation 14)}$$

The SR3 regression introduces an additional auxiliary variable $\boldsymbol{w}$ which is used to relax the optimization problem. Because of the use of an ℓ_1 regularization, the regression becomes sparsity promoting and is able to reduce coefficients ξ_i to 0. As a result the threshold l is no longer a strict threshold, but it is included in the choice of the regularization parameter $\alpha(l)$. Instead an additional hyperparameter, tolerance δ_{tol}, is introduced. Although it is not directly included in the regression, it defines when the outcome of optimization is sufficiently good. Through the choice of hyperparameters, selecting optimal values for them is not intuitive compared to RIDGE regression.

Therefore, first determine which pair of hyperparameters provides all three equations (see Figure 6B). Note that we use a single time trace (with 398 ppp) and a term library that only contains terms occurring in the Goodwin model (see table in the E-SINDy extension). Using this set of models, we use the R^2 score as a goodness-of-fit measure to identify which models provide the best fit. As can be seen from Figure 6B, most models either are not able to describe the provided data ($R^2 < 0$), or the model results in nonphysical dynamics ('fail' - f) and only three models provide a R^2 score higher than 0.9 (shown in Table 2). As can be seen, SINDy-PI is able to discover the true equations for u_t and v_t (with $1/(1+w^{10}) \approx 1/w^{10}$), however, it still struggles with the simpler equation for w_t. Here, SINDy-PI provides approximations of both equations which are able to qualitatively reproduce the dynamical behavior of the studied system (see Figure S6). The correct discovery of the underlying model could be achieved by increasing the amount of data. However, even with a single time series, we are able to at least identify the correct type of nonlinearity (for high resolution, no noise data, small library). This knowledge can then be used to provide a better truncation of the term library for original SINDy. We therefore decided to identify how robust this identification is toward sampling and noise only focusing on how well one can recover the nonlinear Hill function (or its approximation $1/w^{10}$), see Figure 6C. Here, SINDy-PI shows to be highly dependent on sampling, where sufficient resolution is required in order to identify the correct nonlinearity, but when more data are provided identification fails. This results from more ambiguous model identification of the nonlinearity when actual sparsity promoting regression methods are used, which we found not to be dependent on noise (see Figure 6C). At this point, it is important to truncate the SINDy-PI library correctly, as the use of larger libraries can reduce successful identification of the nonlinearity (see STAR methods).

More recently, SINDy has also been used to identify a model describing cancer and CAR T cell dynamics,[53] or population dynamics within an aphid-ladybeetle system[52] using extensive prior knowledge on the nonlinear interactions to provide these in the term library. Beside using SINDy-PI or extensive prior knowledge, another suitable way to determine the nonlinear rational term, is to provide new knowledge about possible nonlinear interactions between components of a biochemical system, which is usually gained from perturbation experiments. See for example the approach for obtaining a model of the tumor suppressor protein p53 in response to DNA damage in Geva-Zatorsky et al.,[14] and of glycolytic oscillations in yeast cells in Nielsen et al.[65] Assuming that we have the knowledge of the nonlinearity in Equation 9, the Hill function can be introduced as an additional term in the term library in SINDy.

However, using SINDy in this way does not lead to the correct identification of the Goodwin model. The reason for this is the random correlation of several terms contained in the library, e.g., u and $uH(v)$ or $uH(u)$ (see Figure 6D). If these terms are present in the optimization problem, the regression algorithm is able to freely choose any coefficient for these terms, since they are almost identical and thus indistinguishable for the problem, e.g., for u and $uH(v)$:

$$\begin{aligned} uH(v) = u\frac{1}{1+v^{10}} \quad &\text{with} \quad \mathcal{O}(v) = 10^{-1} \\ \rightarrow \quad &uH(v) \approx u \cdot 1 \end{aligned} \qquad \text{(Equation 15)}$$

As a result, after initializing the library, it is important to identify any existing correlations between library terms. Two library terms are correlated if the result of the Pearson's product-moment coefficient is $\rho = 1$. However, there is no common threshold ρ_{thres} above which two variables are correlated. We therefore decided to find a ρ_{thres} empirically by observing the distance of the term correlations ρ_{ij} from 1 (see Figure 6E). By applying correlation, we are able to identify the culprits in the library and achieve successful model recovery when a sufficient amount of data (195 ppp) is available (see Figure 6F). However, it should be noted that this method is highly sensitive to noise and requires precise noise filtering, which in itself is a challenge, as we have shown previously.

High dimensionality in the mass action oscillator

For the two models studied so far, we only considered two or three dimensions, where nonlinearities are explicitly expressed either by cubic terms or by the Hill function. In the case of the five-component mass action model the increase in dimensions is able to account for nonlinearity and delay. However, as we have seen from our investigation of experimental systems, despite a simpler representation and a closer relationship to an actual biological system, such an increase can effectively interfere with data-driven model identification. Applying SINDy to the full dataset of a single time series, we observe that more data are required to correctly identify all the underlying equations compared to the previously studied models (2150 ppp in Figures 3B and 7A). Furthermore, we find that the identification with all dimensions present in the data is sensitive to noise and is not successful for our model even when large amounts of ppp are present (see Figure 7A). Increasing the dimensionality of a system may decrease the ability to uncover the underlying dynamics. This is especially true when we have multiple variables acting on scales that are several orders of magnitude apart. As we have pointed out before, these limitations could be potentially

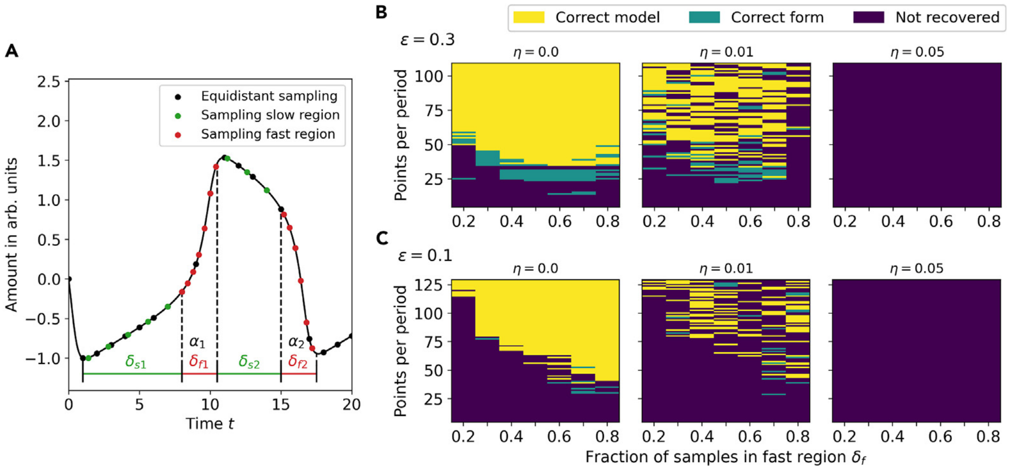

Figure 5. Mitigating timescale separation with optimized sampling

(A) The equidistant sampling can be optimized in order to provide more information on the fast dynamics by distributing the same amount of points unevenly between slow and fast changes.

(B) For timescale separation of $\varepsilon = 0.3$ and by assigning 20% of the time series ($\alpha_1 + \alpha_2 = 0.2T$) the performance is improved if already more then the basic 20% of points are evenly distributed in the fast changes, with an optimal distribution at 50/50 or 60/40 in favor of the fast changes.

(C) For stronger timescale separation of $\varepsilon = 0.1$ an improved sampling strategy is able to significantly reduce the amount of points required, where the performance improves with the amount of points assigned to the fast changes, reducing the required amount from 115 ppp to 40 ppp with a distribution of 80/20.

overcome if the dataset would contain more than one trajectory; however, providing tens or hundreds of trajectories of adequate quality for a high-dimensional system can be challenging. Thus, identifying such high-dimensional systems from all possible states seems highly impractical, even if all relevant variables are measured. We could reduce the number of state variables to the most relevant ones, e.g., by using encoders.[77,78] However, as shown especially in Chen et al.,[78] large amounts of high quality data are needed to identify the most relevant aspects of an observed dynamical system, while the set of variables we provide is also the relevant set of state variables for the model. At this point, we have shown that if there is not too much timescale separation in the data, it is more advantageous to work with lower dimensional data, since a lower sampling resolution is required and SINDy is less sensitive to noise. This would move us away from a more biological model toward a conceptual, higher level representation of the dynamical system (as shown in Figure 2). Even though we would not uncover the actual interactions, we could learn and understand the underlying mechanisms of the system. When studying the BZ reaction (see Figure S3) we have seen that not every reduction of a system is able to provide an interpretable model. Since we have access to all variables of the system, we can test the model identification of every pairwise combination of the state variables u, v, w, x, y. To do this, we center the limit cycles of the various reduced systems around (0,0), since for most generic models the unstable fixed point lies at (0,0) within the limit cycle, and we try to reduce the amount of additional terms that account for an offset (see Figure 7B). We then scan the hyperparameters threshold l and the regularization parameter α over several orders of magnitude and determine the complexity k and the R^2 score of the identified models in Figure 7C. For the scan, we see that we are able to obtain high R^2 scores for three combinations: (u,v), (v,w), and (v,x). In this analysis, we also plot the projected phase space plots of the respective combinations, and we clearly see that when the variables forming the limit cycle are well separated, SINDy is able to identify important dynamical features of the system from the phase space. The only exception is the combination of (v,y) for which SINDy is not able to identify models leading to a high R^2, despite a clear separation in the variables. This is a situation similar to the identification of the BZ reaction in the previous section. Since we have a sharp change in two interacting variables, this change cannot be approximated by a cubic polynomial. For the the mass action oscillator, such sharp changes are shown with a red circle in the phase plot of (v,y) in Figure 7C, and similar behavior is found for the BZ reaction in Figure 1E. In the case of the BZ reaction, polynomials of order 7 or higher were required to obtain a sufficient, but uninterpretable, approximation of the system, and for the mass action oscillator we do not provide such high order terms. This indicates an unfavorable reduction of the mass action system in the (v,y)-space and it requires either an additional variable or knowledge of the type of reduction that leads to this behavior. However, when comparing the results of the R^2 score with the complexity k, we choose the values of the threshold l and the regularization parameter that give the best trade-off between complexity and accuracy for the other well-separated variable combinations. For (u,v) Equation 33 is able to reproduce the dynamical behavior of the reduced system (see Figure S8A and STAR methods). Furthermore, the equations are remarkably close to the FHN equation in Equation 7 and can even be analyzed analytically. With this reduction we are able to create a conceptual understanding of the underlying mass action system without the need for high quality data or the evaluation of all state variables at once.

Similarly the Equations 34 and 35 for the (v,w) and (v,x) respectively, are able to approximate the corresponding behavior in the reduced system (see Figures S8B and S8C). Both equations do not resemble a simple FHN-type equation, since all equations contain terms up to cubic

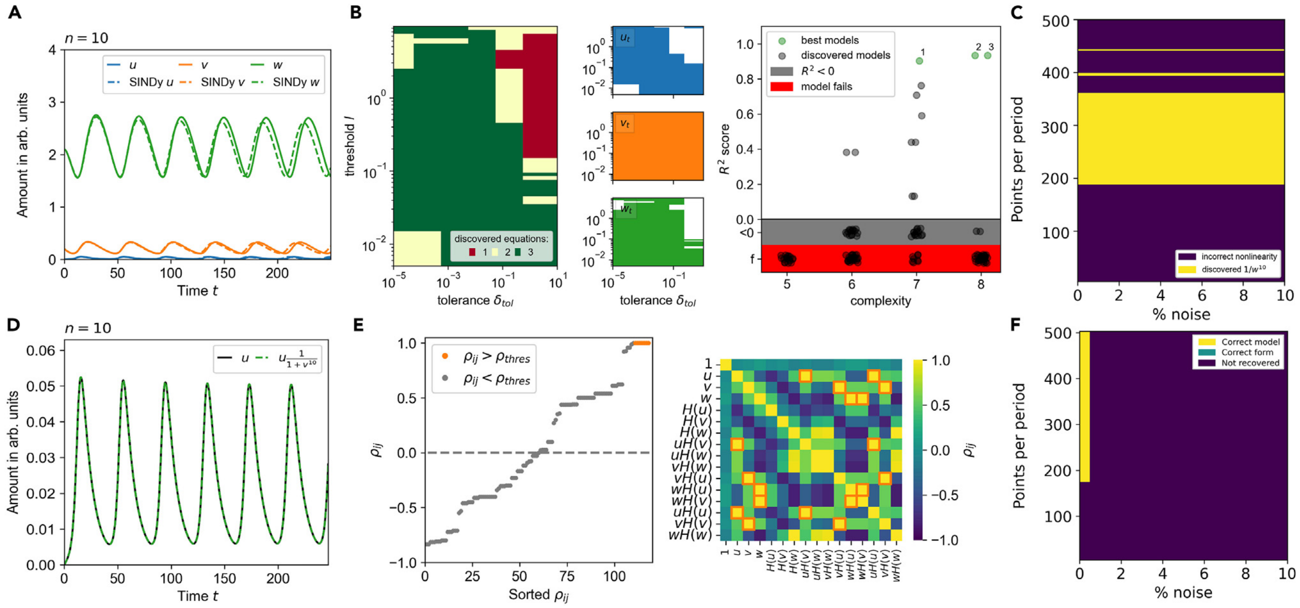

Figure 6. Enabling identification of a Hill-type response function with SINDy

(A) SINDy cannot find the interpretable Hill-function but is able to approximate the nonlinearity ($n = 10$) with higher order polynomials.

(B) SINDy-PI applies the SR3 regression (Equation 14) using the hyperparameters threshold l and tolerance δ_{tol}. Only for a subset of hyperparameters the full set of equations (u_t, v_t, w_t) can be identified (see left panel). Using the R^2 score a majority of models either does not reproduce the data or when simulated show non physical behavior (explosion of values). Three models with $R^2 > 0.9$ (called best, shown in Table 2) provide the nonlinearity $1/w^{10} \approx H(w)$, but do not match the Goodwin model.

(C) Identification of the Hill-function is highly sensitive to data amounts but not toward the amount of noise.

(D) When the Hill functional form is known, SINDy is not able to identify the underlying model because of existent correlations between library terms, e.g., u and $uH(v)$.

(E) Correlations ρ_{ij} between different terms are identified and a threshold ρ_{thres} is applied from which correlated terms are excluded from the term library.

(F) Excluding correlated terms allows SINDy to identify the correct underlying model. However, correlating the term library is only possible for low noise levels.

order. Furthermore, as recently pointed out,[98] a system consisting of two coupled bistable switches, i.e., the nullclines of a two-dimensional system are described by cubic polynomials, may lead to more robust oscillations and may be closer to actual biological reality.

High-order nonlinearities and high dimensionality in model identification (answers to Q4 and Q5)

In the second part of the study, we tried to answer whether different formulations of nonlinearities in oscillatory models beyond the polynomial can be identified using SINDy, in this case evaluating the Hill function. Since SINDy by itself is not able to provide rational terms, i.e., the correct form of the Hill function, it can only provide approximations of the nonlinearity in polynomial form, which may not be interpretable without prior knowledge. Therefore, we evaluated the extension SINDy-PI while applying it only on a single time trace, which reformulates the optimization problem with rational terms in an implicit form. When applying SINDy-PI with a library that is truncated to only contain terms included in the Goodwin model with the order of the nonlinear Hill function $n = 10$ and on high resolution data (398 ppp) with no noise, we are able to discover a set of models that are able to reproduce the provided data. These models are also able to identify the approximated Hill-function (as $1/w^{10}$, but they struggle to provide the correct form for the simpler third equation w_t. Nevertheless, SINDy-PI can be used to determine (if data quality and library truncation are suitable) possible nonlinearities within a model (here $H(w)$ in u_t). This knowledge can be then used to introduce suitable terms into the library for the original SINDy method to uncover the full correct model. Another possibility to discover nonlinearities using SINDy requires additional measurements, i.e., perturbation experiments, or extensive prior knowledge to determine nonlinear interactions and provide them within the term library. We tried this by providing the correct Hill function formulation in the library, which led to an unsuccessful identification, from which we deduced that it is necessary to perform a prior correlation analysis between the library terms. This allowed us to identify possible correlations and thus enable successful model identification. Thus, we have shown and emphasized the importance of truncating the term library by correlation for regression-based model identification (Q4). We then investigated the representation of time delay and nonlinearities in a higher-dimensional system with low-order interactions by applying SINDy to synthetic data from the five-component mass action model. As shown, the identification of this system requires high quality data, since SINDy is not able to handle additional noise in addition to a large number of points per period. As a result, in the previous part we suggested that especially low-data limits and certain noise levels can be overcome by using lower dimensional systems. Using the existing set of relevant state variables, we attempted to infer models of a reduced two-dimensional system by cross-testing all variable combinations. We find that identification is successful when the state variables are well separated in phase space and SINDy is able to unambiguously identify dynamical features. It can be concluded that the identification of high-dimensional systems with SINDy, even with simple low-order interactions and access to all relevant variables, is challenging and requires high quality data. To enable identification, it is advisable to study possible reduced systems from which, depending on the separation and possibly available prior knowledge (to provide good approximations of terms in the reduced system), one is able to learn and even interpret analytically the dynamical behavior using a high-level representation (Q5).

A step-by-step guide to applying SINDy on experimental data

After studying various limiting aspects of SINDy, we now summarize our findings in the form of a step-by-step guide when aiming at model identification with SINDy from oscillatory experimental data in biology. With this guide, shown in Figure 8, we aim not only to systematize our approach to model identification, but also to provide a guide for experimentalists who want to better understand their dynamic biological system through models, without requiring expertise in classical model identification. The steps included in the setup start with a first application of SINDy on experimental data, which is followed by (numbered as in Figure 8).

(1) classical data manipulation techniques not discussed in this work, namely detrending, normalization and rescaling of time series data.[92]
(2) investigating if provided experimental data meets minimal requirements toward temporal resolution (see Section 'length of time series, equidistant sampling, and added noise' and following).
(3) correctly filtering noise without influencing the outcome of model identification (see Section 'noise filtering techniques').
(4) suitable inclusion of more experimental datasets, either by measuring additional time series or optimizing sampling strategies (see Sections 'addressing noise and low-data in equidistant sampling with multiple trajectories' and 'mitigating timescale separation with improved sampling strategies').
(5) investigating if nonlinearities can be identified using SINDy-PI for only one time series, and then implementing it in the original SINDy approach (see Section 'ultrasensitivity in the Goodwin oscillator').
(6) appropriate handling of correlations within the term library when an ultrasensitive response from the system equations is included in the term library (see Section 'ultrasensitivity in the Goodwin oscillator').
(7) an investigation of possibilities to reduce a high-dimensional system of state variables (see Section 'high dimensionality in the mass action oscillator').

If identification is unsuccessful despite following all suggested steps, the reason likely lies in the lack of knowledge about important missing state variables or interactions in the underlying dynamical system: Missing state variables or (nonlinear) interactions can make the identification of interpretable models difficult or even impossible if they cannot be well approximated within a reduced state space. In this situation, other techniques to uncover missing dimensions of a system have to be applied. Nevertheless, using this approach we now return to one of the first experimental examples, namely glycolytic oscillations in yeast, for which we could not identify an underlying mathematical model (38 ppp, $dt = 1s$, see Figure 1) (Temporal resolution retrieved from personal communication with the authors).

We start by shifting the center of the attractor to (0,0), similar to the evaluation of the mass action model, and rescale the data with a min-max normalization (step (1), see Figure 9A, and S9B). These steps improve the identification, but do not lead to an interpretable model. Thus, we turn to one aspect of our study and apply a noise filtering technique, in this case a low-pass filter, since the oscillations do not show strong timescale separation and are mostly sinusoidal (steps (3), see Figures S9C and S9D). With this application, we are able to identify the following model at $\alpha = 1 \cdot 10^{-17}$ and $l = 1 \cdot 10^{-2}$ with $R^2 = 0.7824$ and complexity $k = 15$:

$$\begin{aligned} u_t &= 0.016 - 0.058u - 0.227v - 0.043u^2 - 0.023uv - 0.020v^2 - 0.015u^3 + 0.054v^3, \\ v_t &= 0.017 + 0.181u + 0.061v + 0.034uv - 0.013v^2 - 0.016u^3 + 0.013v^3. \end{aligned} \qquad \text{(Equation 16)}$$

Remarkably, the identified model contains two equations up to the third order, which in turn can be compared to a model consisting of bistable interconnected switches as proposed by Parra-Rivas et al.[98] Due to its form, the equation is not easy to interpret or to study analytically. However, we study the equation numerically and are able to retrieve the nullclines and visualize the behavior in phase space (see Figure 9B). Compared to the well-studied two-component model of glycolytic oscillations, the Selkov model in Equation 6, we see that we identify a more complex description of the interactions, as the equation generates five fixed points (see Figure 9B): An unstable fixed point (UFP) around which the limit cycle of oscillations occurs; two saddle points (or saddle nodes - SN) for high NADH and low ATP, and low NADH and high ATP concentrations/activities; two steady states (stable fixed points - SFP) for low NADH and low ATP, and high NADH and high ATP concentrations/activities. With this, we identify a biologically/biochemically sound model that is able to address the limitations of the Selkov model, already pointed out by Selkov himself[64]: He points out that his simple model is unable to account for experimentally identified steady states, although these have already been described for oscillations in the yeast *Saccharomyces carlsbergensis*.[99] Our data-driven model accounts for this behavior even though we provide almost no prior knowledge. However, our model shows high complexity making it difficult to be interpreted analytically, which as a result from our study we assume to be due to the low temporal resolution (only 38 ppp, step (2)). Therefore, following our decision tree, we must either collect more additional data or improve the resolution of the experimental data used for model identification

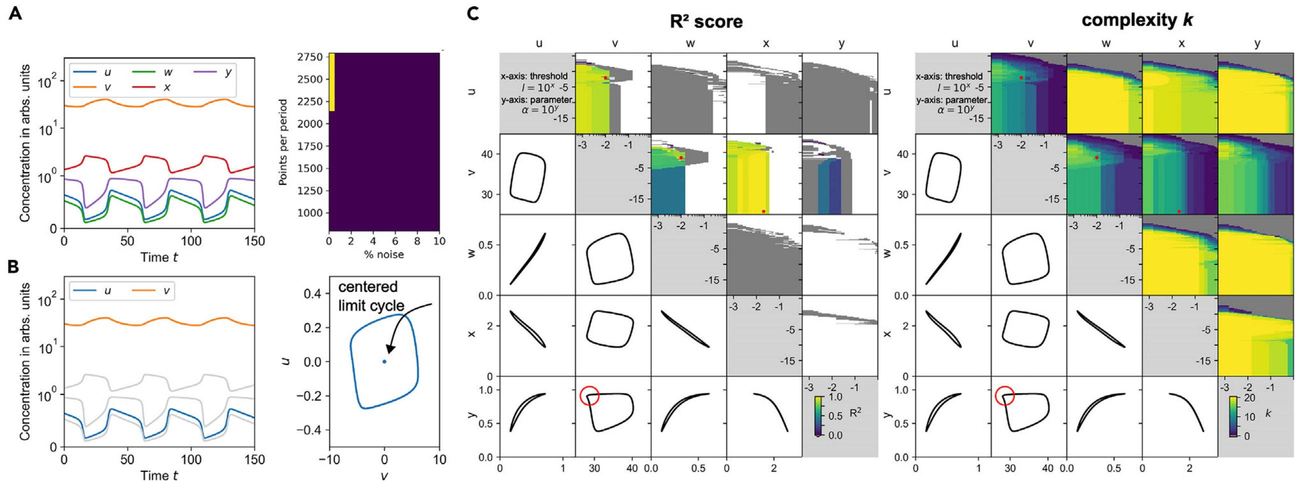

Figure 7. Identification of high-dimensional system by reducing set of state variables

(A) Model identification with high-dimensional data of the mass action oscillator requires high-data/low-noise situation in order to correctly identify the underlying system.

(B) Reducing the system to only two variables, e.g., u and v, and centering the data around the point (0,0), assuming that the unstable fixed point is symmetric toward the limit cycle can be used to derive important dynamical information while reducing data requirements.

(C) Applying SINDy to different combinations of state variables u, v, w, x, y and determining the R^2 score (left) and complexity k (right) within a threshold l and regularization parameter α scan provides us with a set of models with high R^2 scores and low complexity (red dots) that can be further studied dynamically and experimentally. These models occur when the state variables creating the limit cycle are well-separated thus providing sufficient information about the dynamics of the system. Only if the behavior cannot be approximated by a cubic polynomial as for (v, y) (red circle) SINDy struggles to identify a suitable model, similarly as in the BZ reaction.

(step (5)). We suspect that increasing the resolution (either experimentally or even synthetically) could lead to an even simpler model (steps (4) and (5)).

Enhancing identification by synthetically increasing the resolution: An outlook

Since we don't have access to more data, we wanted to try out what impact the application of a simple linear interpolation to our data and synthetically increasing the number of points would have on model identification (step (5)). Increasing the number of points by simple interpolation can be done in this particular case because the oscillations do not have strong timescale separation, however, we do not evaluate the influence of interpolation on data-driven identification.

We increase the number of points by a factor of 10, together with noise filtering, centering and normalizing of the data (see Figure 10 and related to it Figure S9E (increasing resolution), F (noise filtering), G (normalizing), H (normalizing and noise filtering)), and we identify a set of equations that preserves the same dynamical behavior as in the low resolution case while reducing the complexity from $k = 15$ for Equation 16 to $k = 12$ in Equation 36 (for more details see STAR methods). As a results, we assume that by increasing the resolution by a factor of 100 (ca. 3800 ppp, $dt_2 = 0.01$, step (5)), we are able to achieve an even better approximation. As can be seen, we are able to identify a set of different models that represent the highest R^2 scores and thus reproduce the experimental data increasingly well. Here, we choose an equation that gives the best trade-off between R^2 score and identified complexity k, which we find with hyperparameters $\alpha = 1 \cdot 10^{-17}$ and $l = 2 \cdot 10^{-2}$:

$$\begin{aligned} u_t &= -0.032u - 0.224v - 0.025u^2 - 0.052u^3 + 0.049v^3, \\ v_t &= 0.183u + 0.067v - 0.030u^3. \end{aligned} \qquad \text{(Equation 17)}$$

Evaluating how generalizable and/or closely related the model actually is to biological behavior is beyond the scope of this work. However, this analysis shows that by overcoming low-data limits, in this case by using interpolation, the results can lead to accurate and dynamically interesting and qualitatively relevant models that are interpretable. This aspect is an interesting line of work that was shown by Goyal et al.[69] to improve the performance of SINDy when a Runge-Kutta scheme is applied to the input data. However, to our knowledge, there has not been a comprehensive study of this topic in the context of SINDy.

DISCUSSION

In this work, we evaluated why, despite its recent popularity, the SINDy approach for data-driven model identification has rarely been applied to experimental data and has led to the identification of new models directly from experimental data. We focused on the identification of models describing oscillatory systems in biology, which are challenging systems for SINDy due to several factors. We have

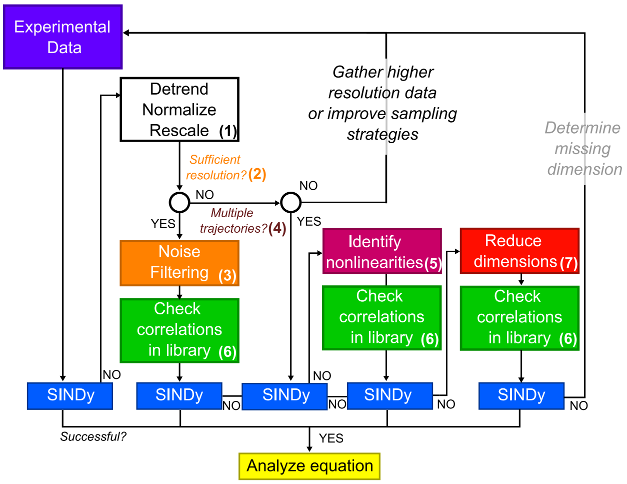
Experimental Data
Detrend
Normalize
Rescale (1)
Gather higher resolution data or improve sampling strategies
Determine missing dimension
Sufficient resolution? (2)
NO
NO
YES
Multiple trajectories? (4)
YES
Noise Filtering (3)
Identify nonlinearities (5)
Reduce dimensions (7)
Check correlations in library (6)
Check correlations in library (6)
Check correlations in library (6)
NO
NO
SINDy
SINDy
SINDy
SINDy
SINDy
NO
NO
NO
NO
Successful?
YES
Analyze equation

Figure 8. Overview of suggested step-by-step approach for application of SINDy on biological oscillator data

Resulting from the study on synthetic data, we suggest a step-by-step guide on how to approach model identification with SINDy when handling oscillatory experimental data in biology.

identified the main challenges by applying SINDy to self-generated or existing experimental data, which are insufficient resolution (or more generally, data availability and quality), high noise levels in experimental measurements, the number of state variables (or dimensions) that fully describe a dynamical system, and limited prior knowledge. We investigated how the first three aspects in particular can influence the outcome of model identification in the special case of biological oscillatory systems. We selected three different oscillatory models (FitzHugh-Nagumo, Goodwin, and a mass action model) capable of representing these challenges and investigated the performance of SINDy. We have also shown that SINDy identification depends on the correct choice of noise filtering technique, and if chosen incorrectly, can obstruct correct identification. To mitigate this, we evaluated the performance of generating more data by either bootstrapping or including more experiments in the analysis and showed that for the special case of oscillatory systems, bootsrapping can reduce SINDy performance and including more data are not able to mitigate strong timescale separation well. At this point, we have also investigated the choice of optimized sampling strategies and have shown that this can improve identification to some extent, although again it does not allow identification for strong timescale separation. We conclude that SINDy struggles especially when the data resolution is low and the oscillatory behavior is characterized by strong timescale separation. Here, identification requires very high resolution or may even be impossible, which is a crucial limitation of SINDy when applied to biological oscillatory data. We then considered the specific aspects of nonlinearity and time delay in biological oscillatory systems, which are represented in the model either by high-order and complex expressions or by an increase in the number of dimensions (state variables). Here, we have shown that for the Hill function commonly used in biochemical models, that the specially developed SINDy extensions SINDy-PI is able to provide knowledge on the approximated nonlinearities when data quality and library truncation is sufficient and SINDy only approximates the behavior with a high-order polynomial. Therefore, when using SINDy, prior knowledge about such high-order interactions must be provided either from SINDy-PI or from additional experiments and the resulting term library must be evaluated for possible correlations between terms to ensure correct identification. For high-dimensional systems, we have shown that even when no noise is applied, SINDy requires large amounts of data to correctly determine the identification. Thus, we have proposed and shown that cross-testing all available datasets of the state variables can enable the identification of a high-level representation of the dynamics in a low-dimensional system. As can be seen from our previous analysis, SINDy needs less data and can handle noise better to provide a suitable model. With this, we were able to identify a set of models that could even be dynamically studied. All these findings have been condensed into a step-by-step guide for model identification with SINDy that can be applied to biological experimental data and beyond. Using our elaborate guide, we were able to enable the identification of an improved model for glycolytic oscillations directly from the original dataset. By pushing the resolution by simple interpolation, we identified an analytically interpretable model of interconnected bistable switches directly from the data. This highlights the need for high resolution data, which is the bottleneck of model identification in general, but especially in biology. Therefore, model identification with SINDy has not yet led to the discovery of new interpretable models. In many cases, increasing the resolution cannot be achieved experimentally, and as we have shown, interpolation can play an important role. In conclusion, we have identified the main limiting aspects of model identification with SINDy when applied to (biological) oscillatory experimental data and propose a step-by-step guide that can improve the identification success. Thus, with this work we aim to encourage the application of SINDy by biological experimentalists and increase the success of model identification directly from experimental data. However, different aspects require further studies to improve the performance of SINDy on experimental data, such as correct normalization and rescaling of data, the generation of more data without additional experiments through interpolation, and the discovery of hidden variables from experimental data.

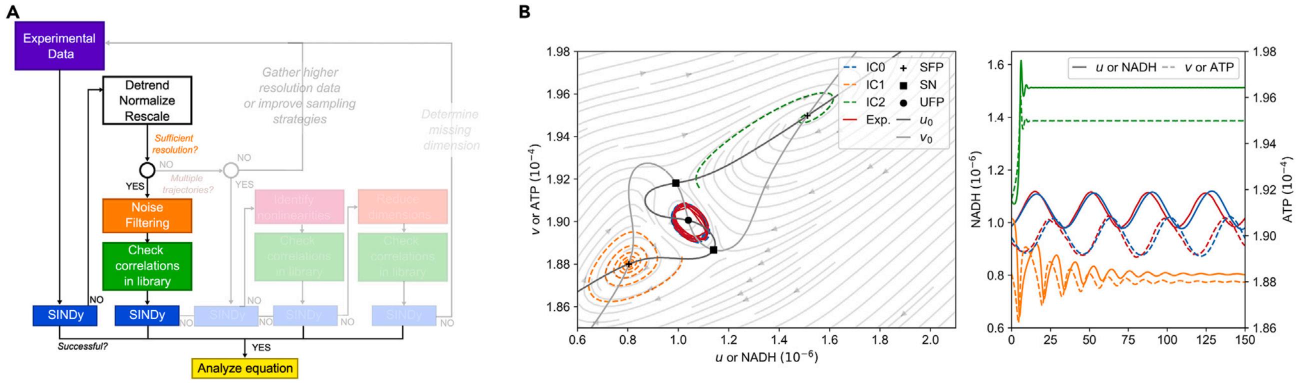

Figure 9. Enabling model identification from experimental data on glycolytic oscillations in yeast

(A) To enable model identification for glycolytic oscillations in yeast, the data are detrended, normalized and centered around (0,0) in phase space. These steps allow us to identify a model which is able to describe the dynamics (Transformed data not shown here).

(B) The found model in Equation 16 with an $R^2 = 0.7824$ and a complexity of $k = 14$ is identified, which is able to describe the dynamical behavior and uncovers steady states in the system that are found in experiments but not represented in the popular Selkov model (Data have been transformed back to be compared to original experimental data; data in right plot uses the same color scheme as the left plot).

LIMITATIONS OF THE STUDY

In our study, we apply simple interpolation in experimental data of the glycolytic oscillator. However, data interpolation is a challenging task in data-driven model identification and SINDy, as if applied incorrectly it can alter the data to represent the result of the interpolation and not the underlying dynamics. Another important aspect that we have not touched on is the correct positioning of the attractor or limit cycle in phase space. In our work, for the sake of simplicity, we centered the limit cycle around the point (0,0), either by removing the offset from the data or by normalization, which in many generic oscillatory models (e.g., FHN) is the unstable fixed point around which oscillations arise. However, even for the FHN model, the point is not positioned symmetrically within the limit cycle, and as we show in other work,[100] correctly positioning the limit cycle in phase space is important for successful model identification. Furthermore, we did not investigate the identification of hidden variables or dimensions directly from experimental data, e.g., in the case of the BZ reaction. The identification of such variables according to the Takens' theorem[101] and delay embedding can significantly improve the success of data-driven model identification[70,79] and result in successful model identification from experimental data.[53] Beside this, we also did not delve into other possibilities to tackle the challenging task of identifying strong nonlinearities like the Hill-function in a dynamical system. An example of such methods is 'Universal Differential Equations'[39] that can be combined with SINDy, to learn 'simpler' (low-order) interactions directly from data and use the strength of neural networks to discover the structure of strong nonlinearities such as the Hill-function. Lastly, we did not carry out a detailed study of SINDy extensions that avoid using derivatives, such as Weak SINDy.[43,102] Here, the authors apply the weak numerical formulation of the problem, which can improve model identification for noisy or timescale separated time series data. We confirmed this as well, see Figure S10. Therefore, a further study of non-derivative based SINDy or other methods that have shown better performance would be useful. These methods could improve model identification for oscillatory systems compared to derivative based SINDy methods.

STAR★METHODS

Detailed methods are provided in the online version of this paper and include the following:

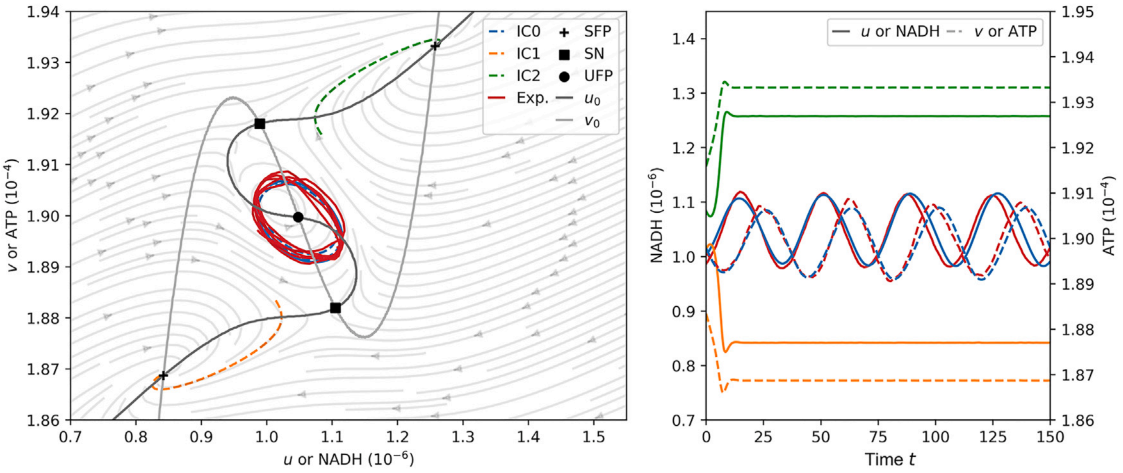

Figure 10. Improving model identification with interpolation of experimental data

Increasing the resolution by 100 times of the original amount of ppp (38 ppp to 3800 ppp) the identified model preserves the dynamical behavior while becoming not only easily interpretable but can also be studied analytically (Data in right plot uses the same color scheme as the left plot).

SUPPLEMENTAL INFORMATION

Supplemental information can be found online at https://doi.org/10.1016/j.isci.2024.109316.

ACKNOWLEDGMENTS

L.G. acknowledges funding by the KU Leuven Research Fund (grant number C14/18/084 and C14/23/130) and the Research Foundation Flanders (FWO, grant number G074321N). We also would like to thank Martina Boiardi, Daniel Cebrian-Lacasa and especially Nikita Frolov for useful discussions and comments.

AUTHOR CONTRIBUTIONS

Conceptualization, B.P. and L.G.; Software, B.P.; Validation, B.P; Formal Analysis, B.P.; Investigation, B.P.; Resources, L.G.; Visualization, B.P.; Writing – Original Draft, B.P. and L.G.; Writing – Review and Editing, B.P. and L.G.; Supervision, L.G.; Funding Acquisition, L.G.

DECLARATION OF INTERESTS

The authors declare no competing interests.

Received: August 31, 2023
Revised: January 18, 2024
Accepted: February 18, 2024
Published: February 23, 2024

REFERENCES

1. Winfree, A.T. (1984). The prehistory of the Belousov-Zhabotinsky oscillator. J. Chem. Educ. *61*, 661.
2. Field, R.J., Koros, E., and Noyes, R.M. (1972). Oscillations in Chemical Systems. II. Thorough Analysis of Temporal Oscillation in the Bromate–Cerium–Malonic Acid System. J. Am. Chem. Soc. *94*, 8649–8664. https://doi.org/10.1021/ja00780a001.
3. Briggs, T.S., and Rauscher, W.C. (1973). An oscillating iodine clock. J. Chem. Educ. *50*, 496. https://doi.org/10.1021/ED050P496.
4. Patke, A., Young, M.W., and Axelrod, S. (2020). Molecular mechanisms and physiological importance of circadian rhythms. Nat. Rev. Mol. Cell Biol. *21*, 67–84. https://doi.org/10.1038/s41580-019-0179-2.
5. Lotka, A.J. (1920). UNDAMPED OSCILLATIONS DERIVED FROM THE LAW OF MASS ACTION. J. Am. Chem. Soc. *42*, 1595–1599. https://doi.org/10.1021/ja01453a010.
6. Volterra, V. (1928). Variations and Fluctuations of the Number of Individuals in Animal Species living together. ICES (Int. Counc. Explor. Sea) J. Mar. Sci. *3*, 3–51. https://doi.org/10.1093/ICESJMS/3.1.3.
7. Murray, A.W., and Kirschner, M.W. (1989). Dominoes and Clocks: the Union of Two Views of the Cell Cycle. Science *246*, 614–621. https://doi.org/10.1126/SCIENCE.2683077.
8. Murari, A., Peluso, E., Lungaroni, M., Gaudio, P., Vega, J., and Gelfusa, M. (2020). Data driven theory for knowledge discovery in the exact sciences with applications to thermonuclear fusion. Sci. Rep. *10*, 19858. https://doi.org/10.1038/s41598-020-76826-4.
9. Huygens, C. (1673). Horologii Oscillatorii. translated by Ian Bruce (2007).
10. Newton, I., Cajori, F., and Motte, A. (1729). Sir Isaac Newton's Mathematical Principles of Natural Philosophy and His System of the World. translated by Andrew Motte.
11. Tyson, J.J. (1977). Analytic representation of oscillations, excitability, and traveling waves in a realistic model of the Belousov–Zhabotinskii reaction. J. Chem. Phys. *66*, 905–915. https://doi.org/10.1063/1.433997.

12. Novák, B., and Tyson, J.J. (2008). Design principles of biochemical oscillators. Nat. Rev. Mol. Cell Biol. *9*, 981–991. https://doi.org/10.1038/nrm2530.
13. Mackey, M.C., and Glass, L. (1977). Oscillation and Chaos in Physiological Control Systems. Science *197*, 287–289. https://doi.org/10.1126/SCIENCE.267326.
14. Geva-Zatorsky, N., Rosenfeld, N., Itzkovitz, S., Milo, R., Sigal, A., Dekel, E., Yarnitzky, T., Liron, Y., Polak, P., Lahav, G., and Alon, U. (2006). Oscillations and variability in the p53 system. Mol. Syst. Biol. *2*, 1–13. https://doi.org/10.1038/msb4100068.
15. Alon, U. (2007). Network motifs: theory and experimental approaches. Nat. Rev. Genet. *8*, 450–461. https://doi.org/10.1038/nrg2102.
16. Glass, D.S., Jin, X., and Riedel-Kruse, I.H. (2021). Nonlinear delay differential equations and their application to modeling biological network motifs. Nat. Commun. *12*, 1788. https://doi.org/10.1038/s41467-021-21700-8.
17. FitzHugh, R. (1961). Impulses and Physiological States in Theoretical Models of Nerve Membrane. Biophys. J. *1*, 445–466. https://doi.org/10.1016/S0006-3495(61)86902-6.
18. Nagumo, J., Arimoto, S., and Yoshizawa, S. (1962). An Active Pulse Transmission Line Simulating Nerve Axon. Proc. IRE *50*, 2061–2070. https://doi.org/10.1109/JRPROC.1962.288235.
19. Goodwin, B.C. (1965). Oscillatory behavior in enzymatic control processes. Adv. Enzyme Regul. *3*, 425–438. https://doi.org/10.1016/0065-2571(65)90067-1.
20. Gonze, D., and Ruoff, P. (2021). The Goodwin Oscillator and its Legacy. Acta Biotheor. *69*, 857–874. https://doi.org/10.1007/s10441-020-09379-8.
21. Agrahar, C., and Rust, M.J. (2022). Optimizing Oscillators for Specific Tasks Predicts Preferred Biochemical Implementations. Preprint at bioRxiv *1*. https://doi.org/10.1101/2022.04.25.489380.
22. Rombouts, J., Verplaetse, S., and Gelens, L. (2023). The ups and downs of biological oscillators: a comparison of time-delayed negative feedback mechanisms. J. R. Soc. Interface *20*, 20230123. https://doi.org/10.1098/RSIF.2023.0123.
23. Otero-Muras, I., Szederkényi, G., Alonso, A.A., and Hangos, K.M. (2012). Inducing sustained oscillations in mass action kinetic networks of a certain class. IFAC Proc. Vol. *45*, 475–480. https://doi.org/10.3182/20120710-4-SG-2026.00147.
24. Ferrell, J.E., and Ha, S.H. (2014). Ultrasensitivity part III: Cascades, bistable switches, and oscillators. Trends Biochem. Sci. *39*, 612–618. https://doi.org/10.1016/J.TIBS.2014.10.002.
25. Miller, G.A. (1956). The magical number seven, plus or minus two: Some limits on our capacity for processing information. Psychol. Rev. *63*, 81–97. https://doi.org/10.1037/h0043158.
26. Leonelli, S. (2019). The challenges of big data biology. Elife *8*, e47381. https://doi.org/10.7554/ELIFE.47381.
27. Tarca, A.L., Carey, V.J., Chen, X.w., Romero, R., and Drăghici, S. (2007). Machine Learning and Its Applications to Biology. PLoS Comput. Biol. *3*, e116. https://doi.org/10.1371/JOURNAL.PCBI.0030116.
28. Loyola-Gonzalez, O. (2019). Black-box vs. White-Box: Understanding their advantages and weaknesses from a practical point of view. IEEE Access *7*, 154096–154113. https://doi.org/10.1109/ACCESS.2019.2949286.
29. Saint-Antoine, M.M., and Singh, A. (2020). Network inference in systems biology: recent developments, challenges, and applications. Curr. Opin. Biotechnol. *63*, 89–98. https://doi.org/10.1016/j.copbio.2019.12.002.
30. Jin, S., Zeng, X., Xia, F., Huang, W., and Liu, X. (2021). Application of Deep Learning Methods in Biological Networks. https://doi.org/10.1093/bib/bbaa043.
31. Li, C., Liu, H., Hu, Q., Que, J., and Yao, J. (2019). A Novel Computational Model for Predicting microRNA–Disease Associations Based on Heterogeneous Graph Convolutional Networks. Cells *8*, 977. https://doi.org/10.3390/CELLS8090977.
32. Park, S.H., Ha, S., and Kim, J.K. (2023). A general model-based causal inference method overcomes the curse of synchrony and indirect effect. Nat. Commun. *14*, 4287. https://doi.org/10.1038/s41467-023-39983-4.
33. Stavroglou, S.K., Pantelous, A.A., Stanley, H.E., and Zuev, K.M. (2020). Unveiling causal interactions in complex systems. Proc. Natl. Acad. Sci. USA *117*, 7599–7605. https://doi.org/10.1073/pnas.1918269117.
34. Raissi, M., Perdikaris, P., and Karniadakis, G. (2019). Physics-informed neural networks: A deep learning framework for solving forward and inverse problems involving nonlinear partial differential equations. J. Comput. Phys. *378*, 686–707. https://doi.org/10.1016/j.jcp.2018.10.045.
35. Cranmer, M.D., Xu, R., Battaglia, P., and Ho, S. (2019). Learning Symbolic Physics with Graph Networks. Preprint at ArXiv *1*. https://doi.org/10.48550/arXiv.1909.05862.
36. Karniadakis, G.E., Kevrekidis, I.G., Lu, L., Perdikaris, P., Wang, S., and Yang, L. (2021). Physics-informed machine learning. Nat. Rev. Phys. *3*, 422–440. https://doi.org/10.1038/s42254-021-00314-5.
37. Lagergren, J.H., Nardini, J.T., Baker, R.E., Simpson, M.J., and Flores, K.B. (2020a). Biologically-informed neural networks guide mechanistic modeling from sparse experimental data. PLoS Comput. Biol. *16*, e1008462. https://doi.org/10.1371/journal.pcbi.1008462.
38. Cranmer, M., Sanchez-Gonzalez, A., Battaglia, P., Xu, R., Cranmer, K., Spergel, D., and Ho, S. (2020). Discovering Symbolic Models from Deep Learning with Inductive Biases. Preprint at ArXiv *1*. https://doi.org/10.48550/arXiv.2006.11287.
39. Rackauckas, C., Ma, Y., Martensen, J., Warner, C., Zubov, K., Supekar, R., Skinner, D., Ramadhan, A., and Edelman, A. (2020). Universal Differential Equations for Scientific Machine Learning. Preprint at ArXiv *1*. https://doi.org/10.48550/arXiv.2001.04385.
40. Billings, S.A. (2013). Nonlinear System Identification (John Wiley & Sons, Ltd). https://doi.org/10.1002/9781118535561.
41. Schmidt, M., and Lipson, H. (2009). Distilling Free-Form Natural Laws from Experimental Data. Science *324*, 81–85. https://doi.org/10.1126/science.1165893.
42. Brunton, S.L., Proctor, J.L., and Kutz, J.N. (2016). Discovering governing equations from data by sparse identification of nonlinear dynamical systems. Proc. Natl. Acad. Sci. USA *113*, 3932–3937. https://doi.org/10.1073/pnas.1517384113.
43. Reinbold, P.A.K., Gurevich, D.R., and Grigoriev, R.O. (2020). Using noisy or incomplete data to discover models of spatiotemporal dynamics. Phys. Rev. E *101*, 010203. https://doi.org/10.1103/PhysRevE.101.010203.
44. Reinbold, P.A.K., Kageorge, L.M., Schatz, M.F., and Grigoriev, R.O. (2021). Robust learning from noisy, incomplete, high-dimensional experimental data via physically constrained symbolic regression. Nat. Commun. *12*, 3219. https://doi.org/10.1038/s41467-021-23479-0.
45. Loiseau, J.-C. (2020). Data-driven modeling of the chaotic thermal convection in an annular thermosyphon. Theor. Comput. Fluid Dyn. *34*, 339–365. https://doi.org/10.1007/s00162-020-00536-w.
46. Hoffmann, M., Fröhner, C., and Noé, F. (2019). Reactive SINDy: Discovering governing reactions from concentration data. J. Chem. Phys. *150*, 025101. https://doi.org/10.1063/1.5066099.
47. Mangan, N.M., Brunton, S.L., Proctor, J.L., and Kutz, J.N. (2016). Inferring Biological Networks by Sparse Identification of Nonlinear Dynamics. IEEE Trans. Mol. Biol. Multi-Scale Commun. *2*, 52–63. https://doi.org/10.1109/TMBMC.2016.2633265.
48. Hirsh, S.M., Barajas-Solano, D.A., and Kutz, J.N. (2022). Sparsifying Priors for Bayesian Uncertainty Quantification in Model Discovery. Royal Society Open Sci. *9*. https://doi.org/10.1098/rsos.211823.
49. Fasel, U., Kutz, J.N., Brunton, B.W., and Brunton, S.L. (2022). Ensemble-SINDy: Robust sparse model discovery in the low-data, high-noise limit, with active learning and control. Proc. Math. Phys. Eng. Sci. *478*. https://doi.org/10.1098/rspa.2021.0904.
50. Prokop, B., Gelens, L., Pelz, P.F., and Friesen, J. (2023). Challenges in identifying simple pattern-forming mechanisms in the development of settlements using demographic data. Phys. Rev. E *107*, 064305. https://doi.org/10.1103/PhysRevE.107.064305.
51. Sandoz, A., Ducret, V., Gottwald, G.A., Vilmart, G., and Perron, K. (2023). SINDy for delay-differential equations: application to model bacterial zinc response. Proc. R. Soc. A A. *479*. https://doi.org/10.1098/RSPA.2022.0556.
52. Anjos, L.d., Naozuka, G.T., Volpatto, D.T., Godoy, W.A.C., Costa, M., and Almeida, R.C. (2023). A new modelling framework for predator-prey interactions: A case study of an aphid-ladybeetle system. Ecol. Inf. *77*, 102168. https://doi.org/10.1016/J.ECOINF.2023.102168.
53. Brummer, A.B., Xella, A., Woodall, R., Adhikarla, V., Cho, H., Gutova, M., Brown, C.E., and Rockne, R.C. (2023). Data driven model discovery and interpretation for CAR T-cell killing using sparse identification and latent variables. Front. Immunol. *14*, 1115536. https://doi.org/10.3389/fimmu.2023.1115536.
54. Gutierrez-Vilchis, A., Perfecto-Avalos, Y., and Garcia-Gonzalez, A. (2023). Modeling bacteria pairwise interactions in human microbiota by Sparse Identification of Nonlinear Dynamics (SINDy). Annu. Int. Conf. IEEE Eng. Med. Biol. Soc. *2023*, 1–4. https://doi.org/10.1109/EMBC40787.2023.10341078.
55. Champion, K., Lusch, B., Kutz, J.N., and Brunton, S.L. (2019a). Data-driven discovery of coordinates and governing equations.

Proc. Natl. Acad. Sci. USA *116*, 22445–22451. https://doi.org/10.1073/pnas.1906995116.

56. Draper, N.R., and Smith, H. (2014). Applied Regression Analysis. Applied Regression Analysis (1–716. https://doi.org/10.1002/9781118625590.

57. Özalp, V.C., Pedersen, T.R., Nielsen, L.J., and Olsen, L.F. (2010). Time-resolved Measurements of Intracellular ATP in the Yeast Saccharomyces cerevisiae using a New Type of Nanobiosensor. J. Biol. Chem. *285*, 37579–37588. https://doi.org/10.1074/jbc.M110.155119.

58. Field, R.J., and Noyes, R.M. (1974). Oscillations in chemical systems. IV. Limit cycle behavior in a model of a real chemical reaction. J. Chem. Phys. *60*, 1877–1884. https://doi.org/10.1063/1.1681288.

59. Tyson, J.J. (1979). Oscillations, Bistability and Echo waves in models if the Belousov-Zhabotinskii reaction. Ann. N. Y. Acad. Sci. *316*, 279–295. https://doi.org/10.1111/j.1749-6632.1979.tb29475.x.

60. Patil, N., Howe, O., Cahill, P., and Byrne, H.J. (2022). Monitoring and modelling the dynamics of the cellular glycolysis pathway: A review and future perspectives. Mol. Metab. *66*, 101635. https://doi.org/10.1016/J.MOLMET.2022.101635.

61. Richard, P. (2003). The rhythm of yeast. FEMS Microbiol. Rev. *27*, 547–557. https://doi.org/10.1016/S0168-6445(03)00065-2.

62. Olsen, L.F., and Lunding, A. (2021). Oscillations in Yeast Glycolysis. In Understanding Complex Systems (Springer Science and Business Media Deutschland GmbH), pp. 211–224. https://doi.org/10.1007/978-3-030-59805-1_13.

63. Bier, M., Bakker, B.M., and Westerhoff, H.V. (2000). How Yeast Cells Synchronize their Glycolytic Oscillations: A Perturbation Analytic Treatment. Biophys. J. *78*, 1087–1093. https://doi.org/10.1016/S0006-3495(00)76667-7.

64. Selkov, E.E. (1968). Self-Oscillations in Glycolysis 1. A Simple Kinetic Model. Eur. J. Biochem. *4*, 79–86. https://doi.org/10.1111/J.1432-1033.1968.TB00175.X.

65. Nielsen, K., Sørensen, P.G., Hynne, F., and Busse, H.-G. (1998). Sustained oscillations in glycolysis: an experimental and theoretical study of chaotic and complex periodic behavior and of quenching of simple oscillations. Biophys. Chem. *72*, 49–62. https://doi.org/10.1016/S0301-4622(98)00122-7.

66. Thaler, S., Paehler, L., and Adams, N.A. (2019). Sparse identification of truncation errors. J. Comput. Phys. *397*, 108851. https://doi.org/10.1016/J.JCP.2019.07.049.

67. Zhang, L., and Schaeffer, H. (2019). On the Convergence of the SINDy Algorithm. Multiscale Model. Simul. *17*, 948–972. https://doi.org/10.1137/18M1189828.

68. Kaiser, E., Kutz, J.N., and Brunton, S.L. (2018). Sparse identification of nonlinear dynamics for model predictive control in the low-data limit. Proc. Math. Phys. Eng. Sci. *474*, 20180335. https://doi.org/10.1098/rspa.2018.0335.

69. Goyal, P., and Benner, P. (2022). Discovery of nonlinear dynamical systems using a Runge–Kutta inspired dictionary-based sparse regression approach. Proc. R. Soc. A A. *478*. https://doi.org/10.1098/rspa.2021.0883.

70. Champion, K.P., Brunton, S.L., and Kutz, J.N. (2019b). Discovery of Nonlinear Multiscale Systems: Sampling Strategies and Embeddings. SIAM J. Appl. Dyn. Syst. *18*, 312–333. https://doi.org/10.1137/18M1188227.

71. Schaeffer, H., and McCalla, S.G. (2017). Sparse model selection via integral terms. Phys. Rev. E *96*, 023302. https://doi.org/10.1103/PhysRevE.96.023302.

72. Lejarza, F., and Baldea, M. (2022). Data-driven discovery of the governing equations of dynamical systems via moving horizon optimization. Sci. Rep. *12*, 11836. https://doi.org/10.1038/s41598-022-13644-w.

73. Delahunt, C.B., and Kutz, J.N. (2022). A Toolkit for Data-Driven Discovery of Governing Equations in High-Noise Regimes. IEEE Access *10*, 31210–31234. https://doi.org/10.1109/ACCESS.2022.3159335.

74. Lagergren, J.H., Nardini, J.T., Michael Lavigne, G., Rutter, E.M., and Flores, K.B. (2020b). Learning partial differential equations for biological transport models from noisy spatio-temporal data. Proc. Math. Phys. Eng. Sci. *476*, 20190800. https://doi.org/10.1098/rspa.2019.0800.

75. Nardini, J.T., Lagergren, J.H., Hawkins-Daarud, A., Curtin, L., Morris, B., Rutter, E.M., Swanson, K.R., and Flores, K.B. (2020). Learning Equations from Biological Data with Limited Time Samples. Bull. Math. Biol. *82*, 119. https://doi.org/10.1007/s11538-020-00794-z.

76. Rega, G., and Troger, H. (2005). Dimension Reduction of Dynamical Systems: Methods, Models, Applications. Nonlinear Dyn. *41*, 1–15. https://doi.org/10.1007/s11071-005-2790-3.

77. Bakarji, J., Champion, K., Kutz, J.N., and Brunton, S.L. (2022). Discovering Governing Equations from Partial Measurements with Deep Delay Autoencoders. Preprint at ArXiv *1*. http://arxiv.org/abs/2201.05136. arXiv:2201.05136.

78. Chen, B., Huang, K., Raghupathi, S., Chandratreya, I., Du, Q., and Lipson, H. (2022). Automated discovery of fundamental variables hidden in experimental data. Nat. Comput. Sci. *2*, 433–442. https://doi.org/10.1038/s43588-022-00281-6.

79. Lu, P.Y., Ariño Bernad, J., and Soljačić, M. (2022). Discovering sparse interpretable dynamics from partial observations. Commun. Phys. *5*, 206. https://doi.org/10.1038/s42005-022-00987-z.

80. Bellman, R. (1954). The theory of dynamic programming. Bull. Amer. Math. Soc. *60*, 503–515. https://doi.org/10.1090/S0002-9904-1954-09848-8.

81. Pitt, J.A., and Banga, J.R. (2019). Parameter estimation in models of biological oscillators: an automated regularised estimation approach. BMC Bioinf. *20*, 82. https://doi.org/10.1186/s12859-019-2630-y.

82. Aliev, R.R., and Panfilov, A.V. (1996). A simple two-variable model of cardiac excitation. Chaos, Solit. Fractals *7*, 293–301. https://doi.org/10.1016/0960-0779(95)00089-5.

83. Nolet, F.E., Vandervelde, A., Vanderbeke, A., Piñeros, L., Chang, J.B., and Gelens, L. (2020). Nuclei determine the spatial origin of mitotic waves. Elife *9*, e52868. https://doi.org/10.7554/ELIFE.52868.

84. Érdi, P., and Tóth, J. (1989). Mathematical Models of Chemical Reactions. Theory and Applications of Deterministic and Stochastic Models (Manchester University Press). https://ui.adsabs.harvard.edu/abs/1989mmcr.book.....E.

85. Hopkins, M., Tyson, J.J., and Novák, B. (2017). Cell-cycle transitions: a common role for stoichiometric inhibitors. Mol. Biol. Cell *28*, 3437–3446. https://doi.org/10.1091/mbc.e17-06-0349.

86. de Boeck, J., Rombouts, J., and Gelens, L. (2021). A modular approach for modeling the cell cycle based on functional response curves. PLoS Comput. Biol. *17*, e1009008. https://doi.org/10.1371/journal.pcbi.1009008.

87. Halley, J.M. (1996). Ecology, evolution and 1f-noise. Trends Ecol. Evol. *11*, 33–37. https://doi.org/10.1016/0169-5347(96)81067-6.

88. Brunton, S.L., and Kutz, J.N. (2022). Data-driven Science and Engineering: Machine Learning, Dynamical Systems, and Control (Cambridge University Press).

89. Ermolaev, A.V., Sheveleva, A., Genty, G., Finot, C., and Dudley, J.M. (2022). Data-driven model discovery of ideal four-wave mixing in nonlinear fibre optics. Sci. Rep. *12*, 12711. https://doi.org/10.1038/s41598-022-16586-5.

90. Corbetta, M. (2020). Application of Sparse Identification of Nonlinear Dynamics for Physics-Informed Learning. In 2020 IEEE Aerospace Conference, pp. 1–8. https://doi.org/10.1109/AERO47225.2020.9172386.

91. Cortiella, A., Park, K.C., and Doostan, A. (2022). A Priori Denoising Strategies for Sparse Identification of Nonlinear Dynamical Systems: A Comparative Study. J. Comput. Inf. Sci. Eng. *23*, 1–34. https://doi.org/10.1115/1.4054573.

92. Kantz, H., and Schreiber, T. (2004). Nonlinear Time Series Analysis, 7 (Cambridge university press).

93. Breiman, L. (1996). Bagging predictors. Mach. Learn. *24*, 123–140. https://doi.org/10.1007/BF00058655.

94. Bühlmann, P.L. (2003). Bagging, subagging and bragging for improving some prediction algorithms. Tech. Rep. Eidgenössische Technische Hochschule (ETH) *1*. https://doi.org/10.3929/ETHZ-A-004483458.

95. Griffith, J.S. (1968). Mathematics of cellular control processes I. Negative feedback to one gene. J. Theor. Biol. *20*, 202–208. https://doi.org/10.1016/0022-5193(68)90189-6.

96. Kaheman, K., Kutz, J.N., and Brunton, S.L. (2020). SINDy-PI: A robust algorithm for parallel implicit sparse identification of nonlinear dynamics: SINDy-PI. Proc. R. Soc. A *476*. https://doi.org/10.1098/rspa.2020.0279. arXiv:2004.02322.

97. Zheng, P., Askham, T., Brunton, S.L., Kutz, J.N., and Aravkin, A.Y. (2019). A Unified Framework for Sparse Relaxed Regularized Regression: SR3. IEEE Access *7*, 1404–1423. https://doi.org/10.1109/ACCESS.2018.2886528.

98. Parra-Rivas, P., Ruiz-Reynés, D., and Gelens, L. (2023). Cell cycle oscillations driven by two interlinked bistable switches. Mol. Biol. Cell *34*. https://doi.org/10.1091/mbc.E22-11-0527.

99. Chance, B., Schoener, B., and Elsaesser, S. (1965). Metabolic control phenomena involved in damped sinusoidal oscillations of reduced diphosphopyridine nucleotide in a cell-free extract of saccharomyces carlsbergensis. J. Biol. Chem. *240*, 3170–3181.

100. Prokop, B., Frolov, N., and Gelens, L. (2024). Data-driven reconstruction of limit cycle position provides side information for improved model identification with SINDy. Preprint at ArXiv *1*. https://doi.org/10.48550/arXiv.2402.03168.

101. Takens, F. (1981). Detecting strange attractors in turbulence. In Dynamical Systems and Turbulence, Warwick 1980, D. Rand and L.-S. Young, eds. (Springer Berlin Heidelberg), pp. 366–381.

102. Messenger, D.A., and Bortz, D.M. (2021). Weak SINDy: Galerkin-Based Data-Driven Model Selection. Multiscale Model. Simul. *19*, 1474–1497. https://doi.org/10.1137/20M1343166.

103. Prokop, B., and Gelens, L. (2024). Replication Data for: ''From biological data to oscillator models using SINDy'' (KU Leuven RDR). https://doi.org/10.48804/SB7TNU.

104. Prokop, B., and Gelens, L.. Gitlab repository. https://gitlab.kuleuven.be/gelenslab/publications/biological_oscillators_sindy(2024).

105. Prokop, B., and Gelens, L. (2024). Code for ''From biological data to oscillator models using SINDy'' (KU Leuven RDR). https://doi.org/10.48804/4INXGQ.

106. de Silva, B., Champion, K., Quade, M., Loiseau, J.-C., Kutz, J., and Brunton, S. (2020). PySINDy: A Python package for the sparse identification of nonlinear dynamical systems from data. J. Open Source Softw. *5*, 2104. https://doi.org/10.21105/joss.02104.

107. Kaptanoglu, A., de Silva, B., Fasel, U., Kaheman, K., Goldschmidt, A., Callaham, J., Delahunt, C., Nicolaou, Z., Champion, K., Loiseau, J.-C., et al. (2022). PySINDy: A comprehensive Python package for robust sparse system identification. J. Open Source Softw. *7*, 3994. https://doi.org/10.21105/joss.03994.

108. Tyson, J.J. (2022). From the Belousov–Zhabotinsky reaction to biochemical clocks, traveling waves and cell cycle regulation. Biochem. J. *479*, 185–206. https://doi.org/10.1042/BCJ20210370.

109. Tyson, J.J., and Fife, P.C. (1980). Target patterns in a realistic model of the Belousov-Zhabotinskii reaction. J. Chem. Phys. *73*, 2224–2237. https://doi.org/10.1063/1.440418.

STAR★METHODS

KEY RESOURCES TABLE

REAGENT or RESOURCE	SOURCE	IDENTIFIER
Deposited data		
Simple pendulum data	This paper	https://doi.org/10.48804/SB7TNU
Belousov–Zhabotinsky reaction data	Field et al.[2]	https://doi.org/10.48804/SB7TNU
Glycolytic oscillation data	Ozalp et al.[57]	https://doi.org/10.48804/SB7TNU
Software and algorithms		
PySindy 1.7	Python library for SINDy, De Silva et al.,[104] Kaptanoglu et al.[105]	https://www.pysindy.readthedocs.io/en/latest/index.html
SciPy 1.7.3	Python library for simulating ODE models	https://www.scipy.org/
Python 3.8.12	Python Software Foundation	https://www.python.org/
Codes for data analysis and visualization	This paper	https://doi.org/10.48804/4INXGQ

RESOURCE AVAILABILITY

Lead contact

Further information and requests for data or code should be directed to and will be fulfilled by the lead contact, Bartosz Prokop (bartosz.prokop@kuleuven.be).

Materials availability

This study did not generate new unique reagents.

Data and code availability

- All experimental or synthetic data have been deposited at RDR by KU Leuven[103] and GITLAB[104], and are publicly available as of the date of publication. DOIs are listed in the key resources table.
- All original code has been deposited at RDR by KU Leuven[105] and GITLAB,[104] and is publicly available as of the date of publication. DOIs are listed in the key resources table.
- Any additional information required to reanalyze the data reported in this paper is available from the lead contact upon request.

EXPERIMENTAL MODEL AND SUBJECT DETAILS

This study did not include experiments with a specific model or subject.

METHOD DETAILS

The SINDy method and its derivatives

In this work we use the original *Sparse Identification of Nonlinear Dynamics* (SINDy), developed by,[42] and extensions of it, which are implemented in the PYTHON package PYSINDY.[106,107] SINDy is based on the assumption that dynamic systems can be described through differential equations in the following form:

$$X_t = N(X, \xi) \qquad \text{(Equation 18)}$$

with a variable $X = (u, v, \ldots)$. The time derivative X_t is a function of the variables X itself, combinations with other state variables and a set of parameters. Differential equations of this form can be also linearly combined, e.g., for component u:

$$u_t = \xi_1 + \xi_2 u + \xi_3 u^2 + \xi_4 uv + \ldots \qquad \text{(Equation 19)}$$

This equation can be rewritten as a row vector containing all combinations and derivatives of the quantity, called the term library and a parameter vector ξ containing all parameters:

$$u_t = \begin{pmatrix} 1 & u & u^2 & uv & \ldots \end{pmatrix} \xi. \qquad \text{(Equation 20)}$$

The values of each term in the library can be calculated from a single shot at a given point in time. If this system is extended to all available time points, a linear system of equations with the unknown parameter vector $\boldsymbol{\xi}$ and the term library matrix $\boldsymbol{\Theta}$ is formed:

$$\begin{pmatrix} u_t \end{pmatrix} = \begin{pmatrix} 1 & u & u^2 & uv & \dots \end{pmatrix} \begin{pmatrix} \xi \end{pmatrix} = \boldsymbol{\Theta\xi} \qquad \text{(Equation 21)}$$

This system poses an over-determined optimization problem for values of $\boldsymbol{\xi}$ and can be solved by using sparsity promoting regression algorithms. In our work we use the RIDGE regression with sequential thresholding optimization algorithm (see Equation 2). We evaluate the performance of SINDy and its extensions mostly using one trajectory (except for the section 'addressing noise and low-data in equidistant sampling with multiple trajectories') with a set random seed to ensure that our results are reproducible.

The E-SINDy extension

Aside of this we also include the recently developed ensemble SINDy extension (E-SINDy) from.[49] Here, the original system of linear equations in Equation 21 is divided in to sets of subsystems, also called bootstrapping. The system can be sub-sampled in two different ways, either row/data wise only including subsets of measured data or column/library wise only including certain terms into sub-libraries into the optimization problem. After solving all the subsystems, the solutions are aggregated and terms or their respective coefficients are assigned with a probability of inclusion. The authors of this approach claim that through bootstrapping application the model identification is more robust in low-data and high-noise regimes and, therefore, poses an optimal extension for our analysis. For the different experimental systems under investigation, suitable term libraries are defined which can be seen in below table.

Table 3. Respective term libraries used for model discovery from experimental data

System	Term library $\boldsymbol{\Theta}$	Range of l	Range of α
Simple pendulum	$\theta, \theta_t, \cos(\theta), \cos(\theta_t), \sin(\theta), \sin(\theta_t)$	$0 - 5$	$10^{-4} - 10^2$
BZ reaction	$1, v, w, v^2, vw, w^2, v^3, v^2w, vw^2, w^3, v^4, v^3w, v^2w^2, vw^3, w^4, v^5, v^4w, v^3w^2, v^2w^3, vw^4, w^5, v^6, v^5w, v^4w^2, v^3w^3, v^2w^4, vw^5, w^6, v^7, v^6w, v^5w^2, v^4w^3, v^3w^4, v^2w^5, vw^6, w^7, v^8, v^7w, v^6w^2, v^5w^3, v^4w^4, v^3w^5, v^2w^6, vw^7, w^8, v^9, v^8w, v^7w^2, v^6w^3, v^5w^4, v^4w^5, v^3w^6, v^2w^7, vw^8, w^9$	$10^{-4} - 7 \cdot 10^1$	$10^{-20} - 6 \cdot 10^{-10}$
Glycolytic oscillations	$1, u, v, u^2, uv, v^2, u^3, u^2v, uv^2, v^3$	$10^{-3} - 10^0$	$10^{-20} - 9 \cdot 10^5$
FitzHugh-Nagumo	$1, u, v, u^2, uv, v^2, u^3, u^2v, uv^2, v^3$	min ξ	10^{-20}
Goodwin (for SINDy)	$1, u, v, u^2, uv, v^2, u^3, u^2v, uv^2, v^3$	min ξ	10^{-20}
Goodwin (for SINDy-PI) reduced library	$1, u, v, w, u^{10}, v^{10}, w^{10}, uv^{10}, uw^{10}, vw^{10}, u_t, v_t, w_t, uu_t, vu_t, wu_t, u^{10}u_t, v^{10}u_t, w^{10}u_t, uv^{10}u_t, uw^{10}u_t, vw^{10}u_t, uv_t, vv_t, wv_t, u^{10}v_t, v^{10}v_t, w^{10}v_t, uv^{10}v_t, uw^{10}v_t, vw^{10}v_t, uw_t, vw_t, ww_t, u^{10}w_t, v^{10}w_t, w^{10}w_t, uv^{10}w_t, uw^{10}w_t, vw^{10}w_t$	$10^{-2} - 10^1$	$10^{-5} - 10^0$ (here δ_{tol})
Goodwin (for SINDy-PI) large library	$1, u, v, w, uv, uw, vw, u^2, v^2, w^2, uvw, uv^2, uw^2, vw^2, u^3, v^3, w^3, u^8, v^8, w^8, uv^8, uw^8, vw^8, u^9, v^9, w^9, uv^9, uw^9, vw^9, u^{10}, v^{10}, w^{10}, uv^{10}, uw^{10}, vw^{10}, u_t, v_t, w_t, uu_t, vu_t, wu_t, uvu_t, uwu_t, vwu_t, u^2u_t, v^2u_t, w^2u_t, uvwu_t, uv^2u_t, uw^2u_t, vw^2u_t, u^3u_t, v^3u_t, w^3u_t, u^8u_t, v^8u_t, w^8u_t, uv^8u_t, uw^8u_t, vw^8u_t, u^9u_t, v^9u_t, w^9u_t, uv^9u_t, uw^9u_t, vw^9u_t, u^{10}u_t, v^{10}u_t, w^{10}u_t, uv^{10}u_t, uw^{10}u_t, vw^{10}u_t, uv_t, vv_t, wv_t, uvv_t, uwv_t, vwv_t, u^2v_t, v^2v_t, w^2v_t, uvwv_t, uv^2v_t, uw^2v_t, vw^2v_t, u^3v_t, v^3v_t, w^3v_t, u^8v_t, v^8v_t, w^8v_t, uv^8v_t, uw^8v_t, vw^8v_t, u^9v_t, v^9v_t, w^9v_t, uv^9v_t, uw^9v_t, vw^9v_t, u^{10}v_t, v^{10}v_t, w^{10}v_t, uv^{10}v_t, uw^{10}v_t, vw^{10}v_t, uw_t, vw_t, ww_t, uvw_t, uww_t, vww_t, u^2w_t, v^2w_t, w^2w_t, uvww_t, uv^2w_t, uw^2w_t, vw^2w_t, u^3w_t, v^3w_t, w^3w_t, u^8w_t, v^8w_t, w^8w_t, uv^8w_t, uw^8w_t, vw^8w_t, u^9w_t, v^9w_t, w^9w_t, uv^9w_t, uw^9w_t, vw^9w_t, u^{10}w_t, v^{10}w_t, w^{10}w_t, uv^{10}w_t, uw^{10}w_t, vw^{10}w_t$	$10^{-2} - 10^1$	$10^{-5} - 10^0$ (here δ_{tol})

(*Continued on next page*)

Table 3. ***Continued***

System	Term library $\boldsymbol{\Theta}$	Range of l	Range of α
Goodwin (for correlation)	$1, u, v, w, H(u), H(v), H(w), uH(v), uH(w), vH(w), vH(u), wH(u), wH(v), uH(u), vH(v), wH(w)$	min ξ	10^{-20}
Mass action	$1, u, v, w, x, y, u^2, uv, uw, ux, uy, v^2, vw, vx, vy, w^2, wx, wy, x^2, xy, y^2, u^3, u^2v, u^2w, u^2x, u^2y, uv^2, uvw, uvx, uvy, u^2, uwx, uwy, ux^2, uxy, uy^2, v^3, v^2w, v^2x, v^2y, vw^2, vwx, vwy, vx^2, vxy, vy^2, w^3, w^2x, w^2y, wx^2, wxy, wy^2, x^3, x^2y, xy^2, y^3$	$10^{-3} - 10^{0}$	$10^{-20} - 9 \cdot 10^{5}$

The choice of libraries is motivated by prior knowledge (trigonometric functions for the simple pendulum, higher order terms in BZ reaction) or the expected behavior (3rd order terms for the glycolytic oscillations in assumption of an FHN type equation and from the Selkov model[64]).

The SINDy-PI method

The SINDy-PI (parallel implicit) is a further extension of the created implicit SINDy extension. The implicit SINDy extension changes the target of the optimization approach in order to account for rational terms in the model identification.[47] An example for Michelis-Menten kinetics is also presented in the examples of the PySINDy package:

$$x_t = 0.6 - \frac{1.5x}{0.3+x}. \qquad \text{(Equation 22)}$$

This equation is not solvable for SINDy, but can be translated into an implicit form that then can be solved with SINDy:

$$x_t = \frac{3}{5} - 3x - \frac{10}{3}xx_t. \qquad \text{(Equation 23)}$$

As this formulation is sensitive to noise,[47,96] the parallel implicit extension solves the SINDy regression problem for all terms as the target of the optimization, e.g., $x_t, x, xx_t, \ldots$.

Analysis of reproducibility using SINDy with random seeds

We analyze the how the outcome of analysis is influence by the choice of random seed in the Python script. Choosing a specific random seed can result in randomness of results, however we see when varying the random seed of calculations that the obtained results (here for FHN with $\varepsilon = 0.3, 0.1, 0.01$) still hold (see Figure S1). This is shown by the distributions which shows minimal amount of points per period required for successful identification for all 50 seeds.

Analysis of simple pendulum

We begin with the oscillations of a simple pendulum system from Figure 1. For this investigation we have generated a video of a swinging brass ball (m = 44 g) attached to a metal wire (L = 0.43 m). During the video the ball is observed over a time t = 12s with dt = 0.008s and oscillates 9 times during the observation time. From literature, the equation describing the oscillations of friction-free simple pendulum defined in polar coordinates of the displacement angle is the following:

$$\theta_{tt}(t) = -\frac{g}{L}\sin(\theta(t)) \qquad \text{(Equation 24)}$$

Using this prior knowledge on the dimensions of the system and a simple convolution neural network, which was trained to detect the ball, we track the displacement of the ball over time and calculate the displacement angle $\theta(t)$. Using the original temporal resolution, we apply the SINDy approach using Ridge regression, scanning over a set of thresholds l and penalizing factors α. The results of the analysis can be seen in Figure S2. After comparing the determined complexity and R^2 score, we select a combination $l = 1.5, \alpha = 10^{-3}$ which combines lowest complexity with the highest adjusted R^2 score (marked in Figure S2). The discovered equation with SINDy and additional application of the small angle approximation leads to the following equations,

$$\begin{aligned} \theta_{tt} &= -24.798\,\theta + 2.071\sin(\theta) - 0.067\sin(\theta_t) \\ &\xrightarrow{\sin(x)\approx x} \theta_{tt} = -22.727\sin(\theta) - 0.067\,\theta_t \end{aligned} \qquad \text{(Equation 25)}$$

This equation has the same form as suggested by theory in Equation 24 with the additionally discovered friction term, $-b/m\,\theta_t$ with b the damping and m the mass of the ball. Interpreting the parameters as in Equation 24 and the additional friction term leads to the following:

$$-\frac{g}{L} = -22.727 \rightarrow L = 0.4316\text{m}, -\frac{b}{m} = -0.067. \quad \text{with} \quad m = 44g \rightarrow b = -2.95\frac{g}{[\text{rad}]} \tag{Equation 26}$$

We have successfully identified the correct equation from experimental data (with which we are able to determine the correct length of the pendulums wire) and also discovered the realistic friction term using the SINDy algorithm. Therefore, as a proof-of-concept in the case of high-resolution, low-noise and prior-knowledge of the mechanism, we are able to identify the underlying governing equations correctly.

Application on BZ reaction data

Data correction of original potentiometric data

In order to hopefully rediscover the underlying Oregonator model from BZ data, we detrended the data using a rolling window mean and additionally rescaled all local maxima and minima of the periods to the maximum and minimum of the first period. With this we wanted to reduce the impact of reagent depletion in the reaction, which causes the levels of bromine ions and cerium to decrease over time. Furthermore to enable the identification of the Oregonator model, we used prior knowledge on the model and adjusted the data according to the original position of the limit cycle from the Oregonator model.

Analysis

Now we can consider the well-studied chemical oscillatory system, the Belousov–Zhabotinsky reaction, one of the earliest studied chemical systems is the Bromate-Cerium-Malonic Acid system, which also led to the formulation of a mechanism describing the emergence of temporal oscillations, called the Field-Körös-Noyes (FKN) mechanism.[2] In this system the main interaction occurs between three compounds: the negatively charged bromine compounds or bromine ions $[\text{Br}^-]$, the positively charged cerium(IV) and cerium(III) ratio $[\text{Ce}^{4+}]/[\text{Ce}^{3+}]$ and the neutral bromous acid $[\text{HBrO}_2]$.[2] Together with potentiometric measurements of bromine and cerium ion concentrations, FKN determined a reduced mechanism that was able to describe the emergence of oscillations. Later, Fields and Noyes have shown that the FKN mechanism can be reduced even further to a set of three ordinary differential equations, also called the Oregonator[58] which brought into the following form by Tyson[59,108]:

$$\begin{aligned} u_t &= p\left[u(1-u) - v(u-q)\right], \\ v_t &= p'(uv + gv - 2fw), \\ w_t &= u - w. \end{aligned} \tag{Equation 27}$$

Here, u, v, w can be assigned to the mentioned compounds, being $u = [\text{HBrO}_2]$, $v = [\text{Br}^-]$ and $w = [\text{Ce}^{4+}]/[\text{Ce}^{3+}]$. However, the concentration of component $[\text{HBrO}_2]$ is not obtainable, as it can not be measured potentiometrically. Therefore, we investigate the reduced system, which means to simplify the Oregonator model in Equation 27 with a steady-state approximation of the u_t equation. Reducing the Oregonator model is commonly done when investigating its dynamical behavior, see e.g.,[11,59,109] in which different equations of the system are approximated as a steady state. Now reducing the system in Equation 27 with $u_t = 0$, leads to the following reduced system,

$$\begin{aligned} v_t &= p'(uv + gv - 2fw), \\ w_t &= u - w. \\ \text{with } u(v) &= \frac{(1-v) + \sqrt{(v-1)^2 - 4q}}{2}. \end{aligned} \tag{Equation 28}$$

As we see the expression of $u(v)$ is not trivial, but what does this mean for the application of SINDy? Assuming, that we do not have this knowledge on the underlying mechanism, applying SINDy naively with a term library containing combinations of v and w up to the fifth order is able to produce models which tend to blow-up. We identify the equations by checking all possible solutions in for different pairs of threshold l and penalty factor α for polynomial libraries of order up to 6 (see Figure S3). We adjusted the parameters of the SINDy approach carefully, aiming on providing models which do not result in a blow-up and we were only able to identify such a model at $l = 0.04, \alpha = 10^{-20}$ with a library containing combinations up to the sixth order:

$$v_t = f\left(v, v^2, vw, v^3, \ldots, vw^4\right),$$

$$w_t = f\left(v, w, v^2, vw, w^2, v^3, \ldots, v^2w^3, vw^4, w^5\right) \tag{Equation 29}$$

When compared to the original time series and the limit cycle of the BZ reaction oscillations in Figure 1, the model is able to reproduce the behavior. With knowledge of the mechanism and also the reduction of the system, we are able to identify that the complexity of the discovered model expresses a Taylor series expansion of the steady state. Although not easily interpretable, the SINDy algorithm was able to quantitatively reproduce the temporal oscillations of the BZ reaction just from experimental data. The oscillations have a similar amplitude, while the period is different as the discovered model oscillates slower than the experimental data. The most striking difference can be seen when comparing the resulting limit cycle to the experimental limit cycle of cerium and bromine: slow changes of both compounds are captured well by the model. However, when the concentration of one compound changes rapidly compared to the other it leads to sharp corners in the limit cycle. These changes are not captured by the discovered model. This shortcoming can be directly linked to the reduction of the underlying system to only two compounds: As comparing the Taylor expansion shows, we only approximate the rapid changes introduced through the behavior of bromous acid or component *u*. Therefore, it becomes clear that not being able to observe all variables of a experimental system can significantly obstruct the correct identification and disallow for an interpretable model, despite capturing the qualitative behavior of the system.

Inferred reduced model of the BZ reaction

To improve readability of the main text, we show here the results of the application of SINDy on the original data after transformation.

$$\begin{aligned}
v_t = {} & 0.392v + 37.79\cdot 10^3 v^2 - 3.682vw - 33.5\cdot 10^9 v^3 + 1.29\cdot 10^6 v^2 w - 76.3vw^2 + 23.86\cdot 10^6 v^2 w^2 \\
& - 129.04vw^3 + 72.37\cdot 10^6 v^2 w^3 + 447.32vw^4, \\
w_t = {} & 66.8v + 0.003w + 649.03\cdot 10^6 v^2 - 262.95\cdot 10^3 vw + 1.84w^2 - 228.81\cdot 10^3 v^3 + 9449\cdot 10^9 v^2 w - 533.88\cdot 10^3 vw^2 \\
& - 4.63w^3 + 35.57\cdot 10^6 v^3 w \quad + 50.76\cdot 10^9 v^2 w^2 + 12.82\cdot 10^3 vw^3 - 186.82w^4 - 3.36\cdot 10^6 v^3 w^2 - 25514.\cdot 10^9 v^2 w^3 \\
& + 39.72\cdot 10^6 vw^4 - 606.31w^5
\end{aligned} \qquad \text{(Equation 30)}$$

The polynomial consists of high order terms that aim on accounting for the reduction of a system by approximating it with a Taylor-series expansion:

$$u(v) \approx \frac{1}{2}\left(\sqrt{1-4q}+1\right) + \frac{1}{2}\left(\frac{-1}{\sqrt{1-4q}} - 1\right)v - \frac{qv^2}{(1-4q)^{3/2}} - \frac{qv^3}{(1-4q)^{5/2}} - \frac{q(q+1)v^4}{(1-4q)^{7/2}} + \mathcal{O}(v^5) \qquad \text{(Equation 31)}$$

Study of noise filtering in low-data, high-noise situations for model recovery

In order to understand the differences in the success of model identification in Figure 3D, we investigated the influence of sampling on the form of noise and performance of the studied noise filtering techniques low-pass filter, Wiener filter, LPSA and Savitzky-Golay filter in Figure S4. The formulations of the noise filtering techniques are taken from Kantz et al.[92] for the low pass filter, Wiener filter and LPSA, and for the Savitzky-Golay filter we reused the code provided in Lejarza et al.[72]

Multiple trajectories and strong timescale separation

We show here the application of the multiple trajectories setup explained in the section 'addressing noise and low-data in equidistant sampling with multiple trajectories' on data from the FHN with a timescale separation $\varepsilon = 0.1$. Similarly to the case shown in Figure 4C we generate datasets with different initial conditions (IC) and try to identify the model form this aggregated data. We find that providing more initial conditions requires high temporal resolution of the data and is only able to identify the correct form of FHN model for noise levels (see Figure S5). Here the averaging of the solution over multiple trajectories underestimates the role of timescale separation in the model and drops terms that are included in the ground truth solution.

Non-polynomial nonlinearity in model formulation - Hill function

We investigate the performance of SINDy for other forms of nonlinearity in the model formulation with the Hill-function. In our analysis, we provide a term library containing terms up to the third order and try to approximate the dynamical behavior of the Goodwin model with $n = 10$. Results of the SINDy approximation for $n = 8$: Results of the SINDy approximation for $n = 10$:

$$\begin{aligned}
u_t = {} & 4.551u + 52.994u^2 + 2.016uv - 3.663uw - 0.104v^2 + 69.809u^3 - 66.216u^2 v \\
& - 42.768u^2 w + 37.525uv^2 - 5.023uvw + 0.894uw^2 + 0.657v^3, \\
v_t = {} & -3.816u + 32.646u^2 + 12.819uv + 5.468uw - 2.519v^2 - 36.703u^3 \\
& - 39.648u^2 v - 24.347u^2 w + 6.167uv^2 - 3.945uvw - 1.718uw^2 + 2.115v^3 + 0.761v^2 w, \\
w_t = {} & 6.798u + 0.796v - 0.105w - 178.464u^2 + 45.158uv - 9.437uw - 1.516v^2 \\
& + 0.380vw + 881.399u^3 - 429.518u^2 v + 117.386u^2 w + 52.729uv^2 - 29.157uvw \\
& + 3.235uw^2 + 0.580v^2 w - 0.110vw^2,
\end{aligned} \qquad \text{(Equation 32)}$$

The resulting model usually contains a large fraction of the suggest terms in the polynomial library, thus making them challenging to interpret yet are able to approximate the behavior of the system well (see Figure 6A). When SINDy-PI is applied, we are able to identify the nonlinear approximation of the Hill-function, $1/w^{10}$ (see Figure S6A), when provided data has sufficient resolution and low-noise, and we provide a term library that only provides relevant terms already included in the underlying model (see Figure 6). We also identify equations for the w_t equation shown in Table 2 which despite their more complicated form are approximations of the dynamics (see Figure S6B). We also tested SINDy-PI with a larger library, for which we are not sure about the structure of the model, still using high resolution (398 ppp) and no noise conditions. Here, similarly to original SINDy the identification suffers from selecting too many possible terms, however it is able to provide functions for all chosen hyperparameter values (see Figure S7). However, all the provided models fail when evaluated numerically which shows that even when using SINDy-PI to provide nonlinear terms for the original SINDy, not only resolution and noise mitigation play an important role but also the correct truncation of the library.

Analysis of different dimensions in mass action model

In section 'high dimensionality in the mass action oscillator', we investigate how dimensionality reduction can enhance model identification with SINDy and here we provide the models identified with the use of Figure 7C and are mentioned in the section. For (u,v) and $l = 10^{-2}, \alpha = 10^{-2}$ we get the following equation:

$$\begin{aligned} u_t &= 0.377u + 0.061u^2 - 6.902u^3 + 0.277u^2 v, \\ v_t &= -3.414u - 0.044v - 0.094uv. \end{aligned} \qquad \text{(Equation 33)}$$

For the other equations (v,w) at $l = 10^{-2}, \alpha = 10^{-2}$ we identify that:

$$\begin{aligned} v_t &= -0.1491 - 0.055v - 4.107w - 0.129vw + 2.347w^2 + 0.025vw^2 + 7.377w^3, \\ w_t &= 0.146vw^2 - 0.193w^3, \end{aligned} \qquad \text{(Equation 34)}$$

and for (v,x) at $l = 2 \cdot 10^{-2}, \alpha = 10^{-19}$ that:

$$\begin{aligned} v_t &= -0.0661 - 0.065v + 1.578x + 0.048vx + 0.125x^2 - 0.650x^3, \\ x_t &= -0.036v + 0.711x - 1.654x^3, \end{aligned} \qquad \text{(Equation 35)}$$

are able to approximate the corresponding behavior in the reduced system (see Figures S8B and S8C).

Analysis of glycolytic oscillations following step-by-step instructions

The data of NADH and ATP has been extracted from Özalp et al.,[57] Figure 2. The data has a resolution of $dt = 1s$ according to personal communication with the authors, and is adjusted for drift, however the time series data is already cleaned from noise in Özalp et al.[57] but reused in Figure 13.2A in Olsen et al.[62] with noise. From Figure 13.2A in Olsen et al.[62] we evaluated that the noise levels present are around 20% of the normal distribution of the data and we therefore add this amount of noise to the experimental data following Equation 11. We take only a part of the full dataset and apply SINDy on it, shown in Figure S9A before and B after noise filtering. Afterward, we center and normalize the dataset and apply SINDy again, with (Figure S9C) and without noise (Figure S9D), which lead to the derivation of Equation 16. For the case of high resolution, we have taken the dataset shown in Özalp et al.[57] in Figure 2 and sampled the data with higher resolution of $dt_1 = 0.25$ (380 ppp, ten times higher resolution), which we examine after detrending and rescaling (step (1)). In order to resemble experimental data we add 20% of Gaussian noise with the same characteristics as the lower resolution data. We then go through the same steps while showing the result at every step: high resolution ($dt = 0.25s$, Figure S9E with noise; Figure S9F without noise) and very high resolution ($dt = 0.01$, Figure S9G with noise; Figure S9H without noise) which lead to Equations 36 and 17. With this increase, we were able to identify the following model at $\alpha = 1 \cdot 10^{-17}$ and $l = 1 \cdot 10^{-2}$ with $R^2 = 0.7824$ and complexity $k = 12$:

$$\begin{aligned} u_t &= -0.023 - 0.018u - 0.274v + 0.032v^2 - 0.081u^3 + 0.124v^3, \\ v_t &= 0.019 + 0.188u + 0.076v + 0.030uv - 0.014v^2 - 0.027u^3 \end{aligned} \qquad \text{(Equation 36)}$$

This model with a reduced complexity preserves the previously identified dynamical behavior, comparable to the one with very high resolution in Figure 10 (data not shown here).

Initial study on performance of Weak-SINDy for oscillatory systems

We have also analyzed in an initial study how the Weak-SINDy method[43,102] performs when applied on data from the FHN model with different levels of timescale separation (see Figure S10). As the the Weak SINDy does not use any derivatives but the integral form of the SINDy optimization problem, it also shows improved performance for strong timescale separation.

Libraries used for SINDy

For the analysis of synthetic and experimental data with SINDy, we have used the following combinations of term libraries and hyperparameters listed in the table in the E-SINDy extension.

Evaluation of experimental data

For the evaluation, we look at two parameters: the complexity of the equation and the R^2 score, which we use as a goodness-of-fit parameter. The R^2 score is a commonly applied indicator on the goodness-of-fit of a model derived with regression methods. We apply the R^2 score in the following form,

$$R^2 = 1 - \frac{\sum_i (X_i - F_i)^2}{\sum_i (X_i - \overline{X}_i)^2}, \qquad \text{(Equation 37)}$$

where the numerator expression describes the residual sum of squares and the denominator expression the total sum of squares which are calculated with the original dataset X_i and the respective model $X_{i,t} = F_i(\mathbf{X})$.

Evaluation of synthetic data

We evaluate the performance of the respective SINDy methods by comparing the structure of the candidate models (CM) to the ground true (GT) models provided. We evaluate them under two aspects: if the model has been correctly identified where we accept and relative error in the coefficients $\boldsymbol{\xi}$ which is less than 2%:

$$\epsilon_{ij} = \frac{\xi_{ij,\mathrm{GT}} - \xi_{ij,\mathrm{CM}}}{\xi_{ij,\mathrm{GT}}} < 0.02 \qquad \text{(Equation 38)}$$

Or if the coefficients lie beyond this 2% threshold but the model still has the same mechanistic form as the ground true model. We evaluate these aspects for model specific sampling ranges where we add Gaussian noise between 1 and 10%.